Numerical Simulation of Surface Effect Ship Characteristics and Dynamics

Colton Gager Clark

Thesis submitted to the faculty of Virginia Polytechnic Institute and State University in partial fulfillment of the requirements for the degree of

Master of Science

In

Ocean Engineering

Wayne L. Neu

Alan J. Brown

Leigh S. McCue-Weil

11 September 2014

Blacksburg, VA

Keywords: Surface Effect Ship, Computational Fluid Dynamics, Air Cushion, Free Surface

Numerical Simulation of Surface Effect Ship Characteristics and Dynamics

Colton Gager Clark

ABSTRACT

The use of computational fluid dynamics to investigate surface ship dynamics and characteristics has been growing during recent years. With technological advancements continuing in leaps and bounds more and more complex simulations are possible. The interests of this paper concern the numerical simulations of a surface effect ship which is a specific type of air cushion vehicle. The simulation work presented here attempts to replicate the model tests involving a generic surface effect ship and demonstrate the value of numerical simulations in understanding air cushion vehicles. The model tests consist of a surface effect ship running through a range of Froude numbers in calm seas and a variety of wave cases. The numerical simulations were developed using CD-adapcos's STAR-CCM+ to model the surface effect ship characteristics and dynamics. The pressurized air cushion and flexible, dynamic seals are of the greatest importance when modeling a surface effect ship; however, some idealizations had to be made. The air cushion fans are represented as constant momentum sources while the seals are represented as shortened and rigid. Throughout the simulations drag, pitch, and heave were constantly monitored for comparison purposes with the model tests. It was found that the rigid skirt approximation accounts for a large portion of error when comparisons were made between the numerical and analytical data. Furthermore, it would be impossible to accurately represent the surface effect ship dynamics in waves with this approximation. An alternative method to modeling the skirts was investigated which would include the use of a porosity function. It was found that the porosity skirt model would allow for cushion pressure to be maintained while limiting the interaction of the rigid skirt and the free surface. The full implementation of porous skirts on the surface effect ship is a difficult challenge as numerical instabilities arise. However, implementing the porous skirt would lead to more accurate calm water simulations and the ability to model the surface effect ship in wave cases.

Table of Contents

List of Figures

List of Tables

Nomenclature

U	Characteristic velocity
g	Gravitational constant
L	Characteristic length
v	Craft velocity
Δx	Local grid size
Δt	Time step
R_k	Convergence ratio
r_k	Parameter refinement ratio
S_k	Solution level
ε_k	Difference between solution levels
p_k	Observed order of accuracy
δ_{RE}	Generalized relative error
h	Normalized grid spacing
Δp	Pressure
v_n	Normal velocity
α	Porous inertial resistance
β	Porous viscous resistance

Abbreviations

ACV	Air cushion vehicle
CFD	Computational fluid dynamics
CFL	Courant Friedrichs Lewy number
DOF	Degree of freedom
FEA	Finite element analysis
FN	Froude number
FVM	Finite volume method
HRIC	High resolution interface capturing scheme
MASK	Maneuvering and seakeeping
NSWCCD	Naval Surface Warfare Center Carderock Dvision
RANS	Reynolds-averaged Navier-Stokes
SES	Surface effect ship
T-Craft	Transformable Craft
VOF	Volume of fluid

1. Introduction

The Transformable Craft (T-Craft) was a new ship concept being designed in order to exceed current limitations of amphibious landing craft. These limitations include speed, range, and load capacity. This concept ship should be capable of transforming and operating as three unique types of ships; catamaran, surface effect ship (SES), and an air cushion vehicle (ACV). While all three of these craft type have distinctive capabilities and limitations, the focus of this thesis is on the surface effect ship type. While the T-Craft is a concept ship that may never exist, research presented here contributes to the advancement in understanding of air cushion craft in general. Surface effect ships are a class of air cushion vehicles with rigid side hulls in a catamaran configuration. Flexible seals are located across the bow and stern as well as transversely across the middle of the craft. These flexible skirts are used to capture the cushion pressure created by the large blowers. With the decreased inner draft and additional lift provided by the cushion pressure the SES can operate at high speeds. Through numerical simulations the dynamics of the SES can be observed and characteristic values such as drag can be calculated. The primary are of interest of the research presented here focus on wave effects and so results of these simulations were compared to experimental data of a notional SES model obtained at the Naval Surface Warfare Center, Carderock Division (NSWCCD). Results of the experiments performed at NSWCCD are given by Bishop et al. [1]. In this study, the model craft is simulated in the commercial CFD code STAR-CCM+ and numerical analysis results are compared to experimental results. The focus of this work is on numerical simulations of SES especially pertaining to numerical simulation of wave cases. Through numerical simulations the dynamics of the SES were observed and characteristic values such as drag were calculated. Of primary interest for this study is the simulation of waves in a numerical simulation and the challenges faced when simulating a SES in waves. The goal was to compare experimental trials of a surface effect ship with numerical simulations of a SES operating in a multitude of wave cases.

1.1 Air Cushion Theory

The primary design feature behind the surface effect ship concept is the pressurized cushion of air trapped between the twin hulls and the water surface, the lifted body then has decreased contact with the free surface. The important drag components of a SES are those due to friction with immersed components such as sidewalls, skirts, propellers, rudders, and other appendages. As well the wave-making drag due to the side hulls and moving cushion pressure field are important. Additionally, momentum drag due to the acceleration of the air used for the supporting air cushion, and aerodynamic profile drag of the SES must be taken into consideration at higher speeds accordingly from Yun and Biault [2]. As well, there has been some investigation of SES resistance components within numerical simulations as presented in Maki [3]. All of these drag components must be considered as the surface effect ship is investigated using computational methods.

2. Surface Effect Ship Model

The Naval Surface Warfare Center Carderock Division (NSWCCD) completed model testing of a generic T-Craft design in 2008. The model SES was designed by John Hoyt, and was built in the NSWCCD model shop, model number 5887, as described in Bishop [4]. The SES model featured rigid side hulls with finger type bow and transverse seals while the aft seal is a double lobe type. The cushions are pressurized by two four inch blower fans. Figure 1 shows the SES stationary on cushion in water. Figure 2 shows the skirt configuration on the underside of the craft. Table 1 gives the SES model characteristics.

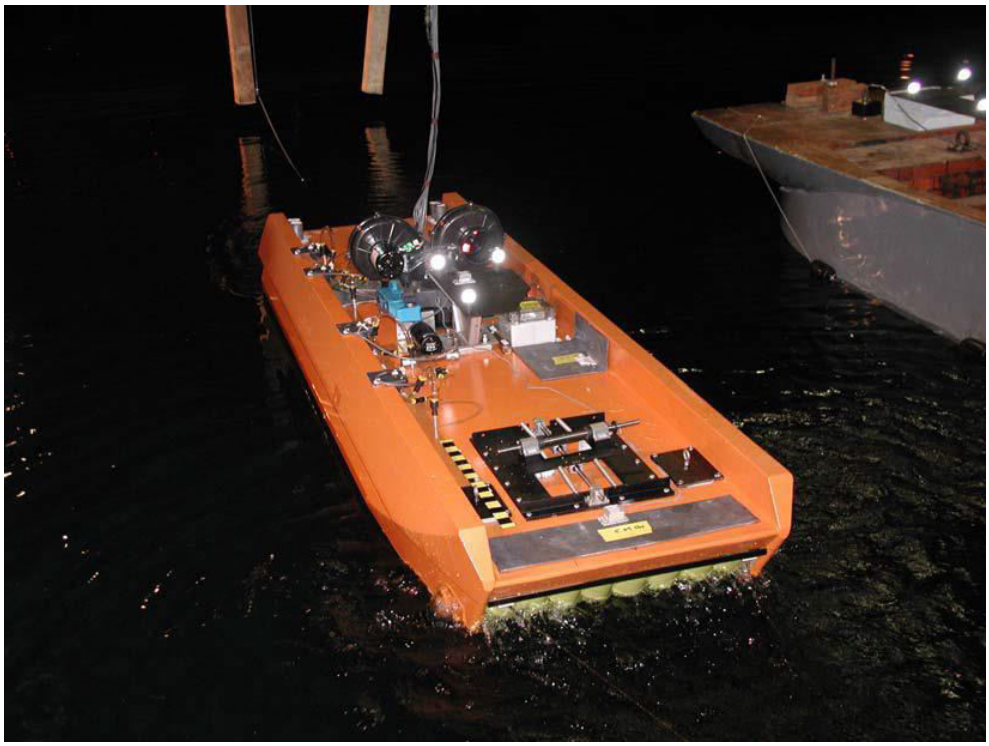

Figure 1: SES model number 5887, Bishop [1].

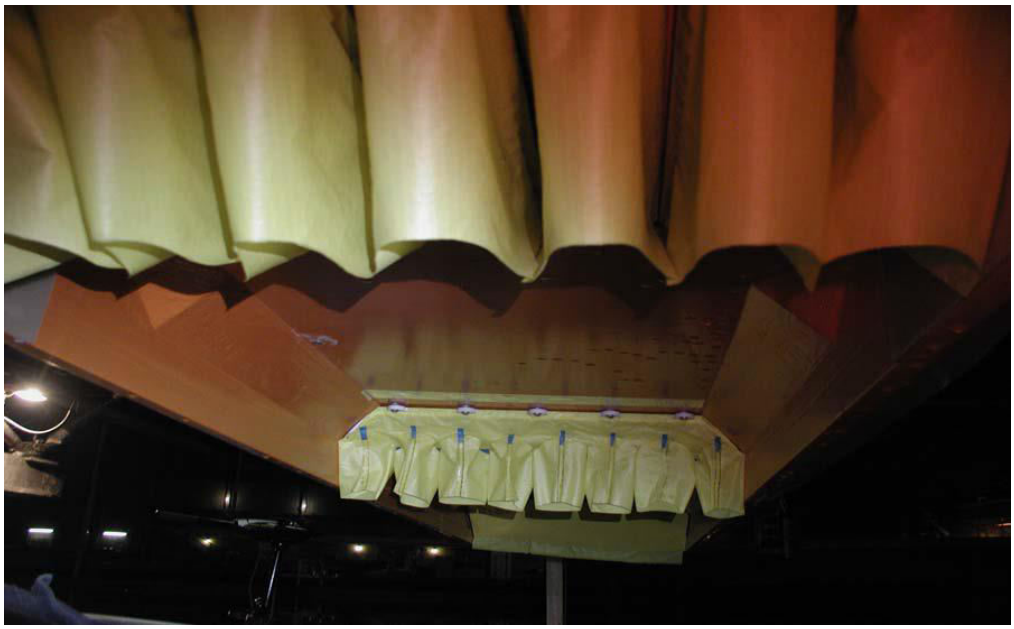

Figure 2: SES skirt configuration, Bishop [1].

Table 1: SES model characteristics.

SES Model Characteristics	
Linear Scale	1: 30.209
Length Overall	99.5 in, 2.5273 m
Length Waterline (off cushion)	98 in, 2.4892 m
Length Waterline (on cushion)	88 in, 2.352 m
Beam Max	29 in, 0.7366 m
Cushion Width	21.5 in, 0.5461 m
Cushion length	87.5 in, 2.2225 m
Displacement	119 lbs FW, 54 kg – (121.5 lbs from report)
LCG, forward of wet deck transom	48.49 in, 1.231646 m
TCG	0.00 in
VCG, below deck	0.09 in, 0.0023 m (0.25 in from report)
GML	18.6 in
Moment of Inertia in Pitch	20.566 slugs-ft2
Moment of Inertia in Roll	2.782 slugs-ft2
Radius of gyration in Pitch	28.44% 2.36 ft
Radius of gyration in Roll	42.25% 0.87 ft
Roll period, model scale from roll decay test	3.66 sec

2.1 Model Tests

Experimental trials were performed at NSWCCD's Maneuvering and Seakeeping (MASK) facility. The MASK facility features pneumatic wave makers on two sides of the basin and a rotating bridge allowing any heading in waves. The model tests were conducted in calm seas and numerous wave conditions. The test conditions considered the SES model at a variety of speeds, wave conditions, and air cushion pressures describe in Bishop [1]. Previous research work has been completed using STAR-CCM+ to replicate some of the model tests performed at NSWCCD. It has been seen in previous numerical simulation work involving surface effect ships, Donnelly [5], that desirable results are possible within STAR-CCM+. The CFD simulations of the given SES model presented here attempt to continue to expand upon that progress.

3. Numerical Simulation

The commercial CFD code STAR-CCM+ by CD-adapco was used to perform numerical simulations of the SES model. STAR-CCM+ is a finite volume method (VFM) code and uses a volume of fluid (VOF) method to model the free surface. In the VOF method, an additional equation is required to describe the transport of scalar volume fractions through the domain. Convective terms of the volume fraction transport equation are discretized using a high resolution interface capturing (HRIC) scheme suited for tracking sharp interfaces according to Muzaferija [6]. The VOF model description assumes that all immiscible fluid phases present in a control volume share velocity, pressure, and temperature fields.

The simulations involving the SES were run both as inviscid and with viscosity enabled. The governing equations for the inviscid simulations are the Euler equations. These equations include a continuity equation and momentum equation for each of the three dimensions. Solving these equations will generate local pressure and velocity components of the fluid. When viscous simulations are used the Reynolds-averaged Navier-Stokes (RANS) equations, which include a viscosity term, are solved. The Spalart-Allmaras turbulence model is implemented in order to determine the turbulent viscosity. Water is modeled as an incompressible fluid while air is modeled separately as an ideal compressible gas. A segregated flow solver is used to solve the governing equations. A second-order upwind convection scheme is used in the segregated flow solver and the linkage between the momentum and continuity equations is achieved with a predictor-corrector approach. Additional information involving computational methods for fluid dynamic problems can be found in Ferziger and Peric [7].

The six degree of freedom solver (6-DOF) allows for the calculated motion of a rigid body in response to the forces and moments imposed on the body by the computed fluid flow. For this study only two motions are examined and the body is restrained in the other four. The SES is allowed to translate vertically in heave and rotate in pitch. As the body moves the entire domain is allowed to move with the body fixed coordinate system in order to maintain the mesh, while the flow remains moving in the global coordinates. An implicit unsteady approach was

used with a first-order temporal discretization with a time step of 0.0025 seconds. In the implicit unsteady approach, each physical time step involves twenty inner iterations to converge the solution for the given time step. The time step was limited based upon the Courant Friedrichs Lewy (CFL) number as given by Equation 1.

$$CFL = \frac{U\Delta t}{\Delta x} \tag{1}$$

The CFL defines a dimensionless relationship between the flow velocity U, local grid size Δx, and the time stepΔt. The CFL number was maintained as a value less than one, so no more fluid may enter a given cell than is available in the upwind cell during each time step. It is possible for simulations with larger CFL to produce solutions but they will not be time accurate.

The computational domain uses a three dimensional half model of the SES with a symmetry plane down the centerline of the SES model. The domain is a rectangular prism that extends in front of and behind the body as well as above and below. The computational domain was kept relatively small to reduce computational cost which may accuracy in the far field. However, the free surface effects under the cushion and around the side hulls should still be resolved accurately. The entire computational domain can be seen in Figure 3. The top and aft faces are pressure outlets while the forward, bottom, and side faces are velocity inlets. The volume fraction, velocity, and pressure setting are all initialized on these faces by the VOF model. Figure 4 shows the interior of the computational domain including the free surface. The free surface needs to be refined enough in order to accurately resolve the flow around the SES. The SES skirts are modeled as rigid in these simulations and shortened so that they capture the cushion pressure but do not drag in the water. The fans that provided the cushion pressure are modeled as momentum sources. These momentum sources work to keep the cushion pressure fixed by pushing air in or out of the cushion. The pressure is initially set based on the SES model data. The full geometry of the SES can be seen in Figure 5.

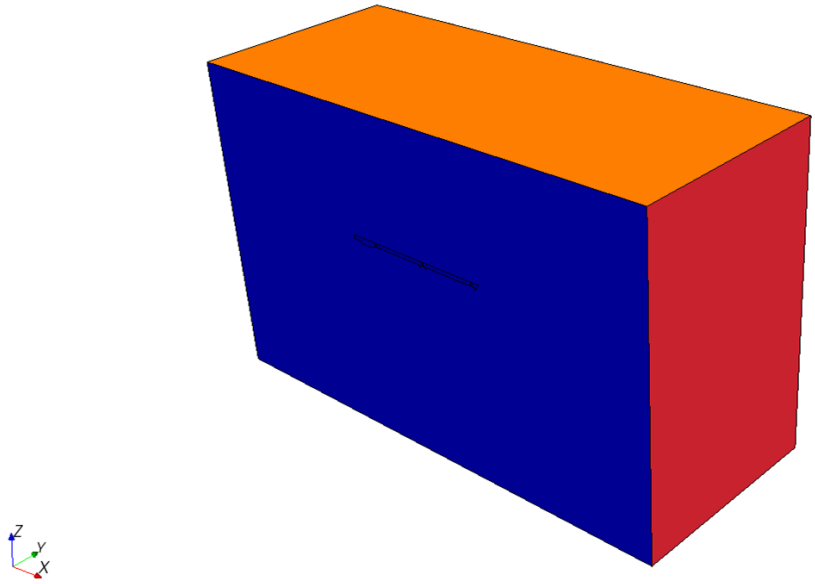

Figure 3: Computational domain; pressure outlet (orange), velocity inlet (red), and symmetry plane (blue).

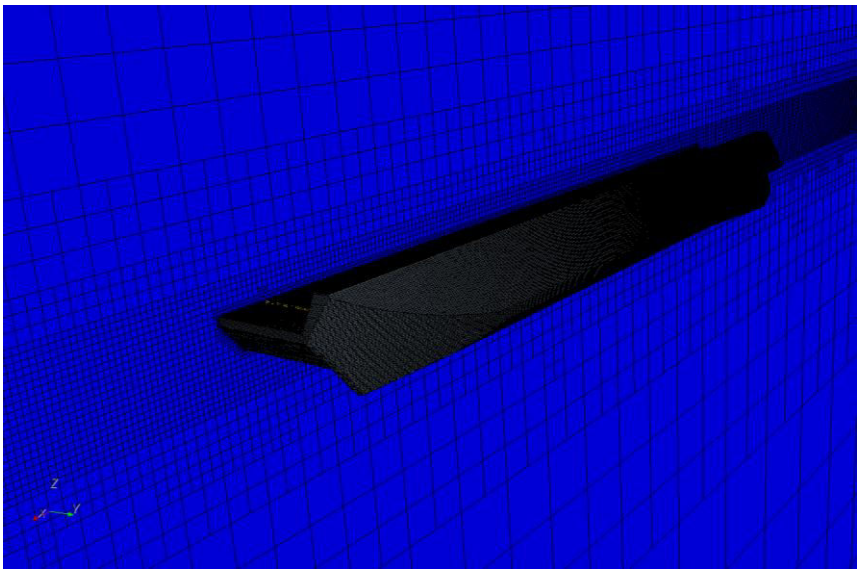

Figure 4: Interior of computational domain with SES half model.

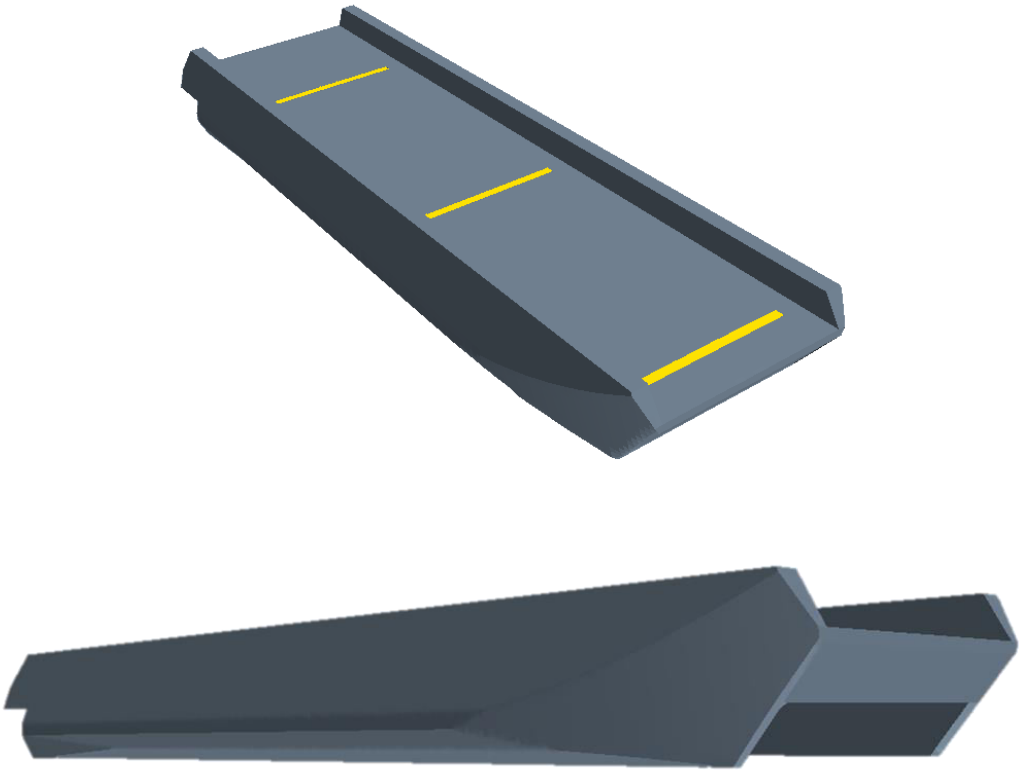

Figure 5: Three dimensional perspective of the SES geometry.

3.1 Air Cushion Modeling and Idealizations

A primary concern when dealing with air cushion vehicles (ACV) is the internal pressurized air cushion that is trapped between the water and the hull of the lifted body. This is especially true when modeling an ACV in a numerical simulation. Without an accurate representation of the pressurized air cushion the full SES cannot hope to be simulated correctly. Fully modeling the fans and blowers that would provide air flow into the pressurized cushion would be a daunting task, therefore, a couple idealizations were made. The determination was made that simply maintaining accurate cushion pressure would be sufficient. Following Donnelly [5], the fans were represented as momentum sources. The momentum sources were used to maintain a cushion pressure that is equivalent to that used during model tests. These momentum sources add a constant value of momentum through a defined volume and in a desired direction. The momentum sources work to keep the cushion pressure fixed by pushing an unlimited amount of air into or out of the air cushion as the cushion pressure decreases or increases from the desired value determined from the model tests which can be found in Bishop [1]. In this way the SES can ride on a pressurized cushion of air that is constantly adjusted in order to ensure accurate modeling of the craft characteristics and dynamics.

4. Grid Refinement Study Involving Inviscid Simulations

Initially the simulations of the SES were run as inviscid. A single grid technique applies a hexahedral mesh to the fluid domain and SES geometry. In order to calculate an accurate solution the computational domain must have an adequately refined mesh so that the fluid flow is resolved correctly. To determine what the correct mesh resolution should be a grid convergence study was performed on a series of systematically refined meshes. The drag on the craft was monitored on these differing meshes and compared in order to determine convergence. During these simulations only the steady state drag was of interest so the time accuracy of the solutions was not of concern.

In order to perform a convergence study for this steady state simulation, using at least three solutions, a systematic parameter refinement by varying the mesh size is needed. The grid size for the fine mesh is coarsened by a factor of the square root of two ($\sqrt{2}$) in order to determine a medium mesh. The coarse mesh is then determined by multiplying by the same factor again. During the course of this study it was determined that the solution converged in an oscillatory manner so two more meshes sizes were run. The fine-medium and medium-coarse meshes complete a series of five symmetrically refined grids with a refinement factor of ($\sqrt[4]{2}$). The mesh specifics can be seen in Table 2. The base size is the largest cell size allowed in the domain. The volumetric control is used to refine the entire waterline. The surface size is specified on the surface of the craft. All of these simulations were performed at a Froude number of 0.6 where the Froude number is defined as a dimensionless ratio between the body's inertial and gravitational forces as seen in Equation 2.

$$Fn = \frac{v}{\sqrt{gL}} \tag{2}$$

Here v is the craft velocity, g is the gravitational constant, and L is the cushion length of the SES. For a simulation involving the SES with a Froude number of 0.6, a velocity of 2.786 meters per second is specified. During the course of these runs the drag was monitored for the half-model. The coarse mesh domain can be seen in Figure 6. These coarse mesh results were compared to four other drag results including the finely meshed domain shown in Figure 7.

Table 2: Mesh refinement specifics.

(m)	Fine	Fine-Medium	Medium	Medium-Coarse	Coarse
Base Size	2	2.378414	2.828427	3.363585	4
Volumetric Control	0.02	0.023784	0.028284	0.036358	0.04
Hull Surface Size	0.01	0.011892	0.014142	0.016817	0.02
Number of Cells	2570982	1809430	1047877	736768	425658

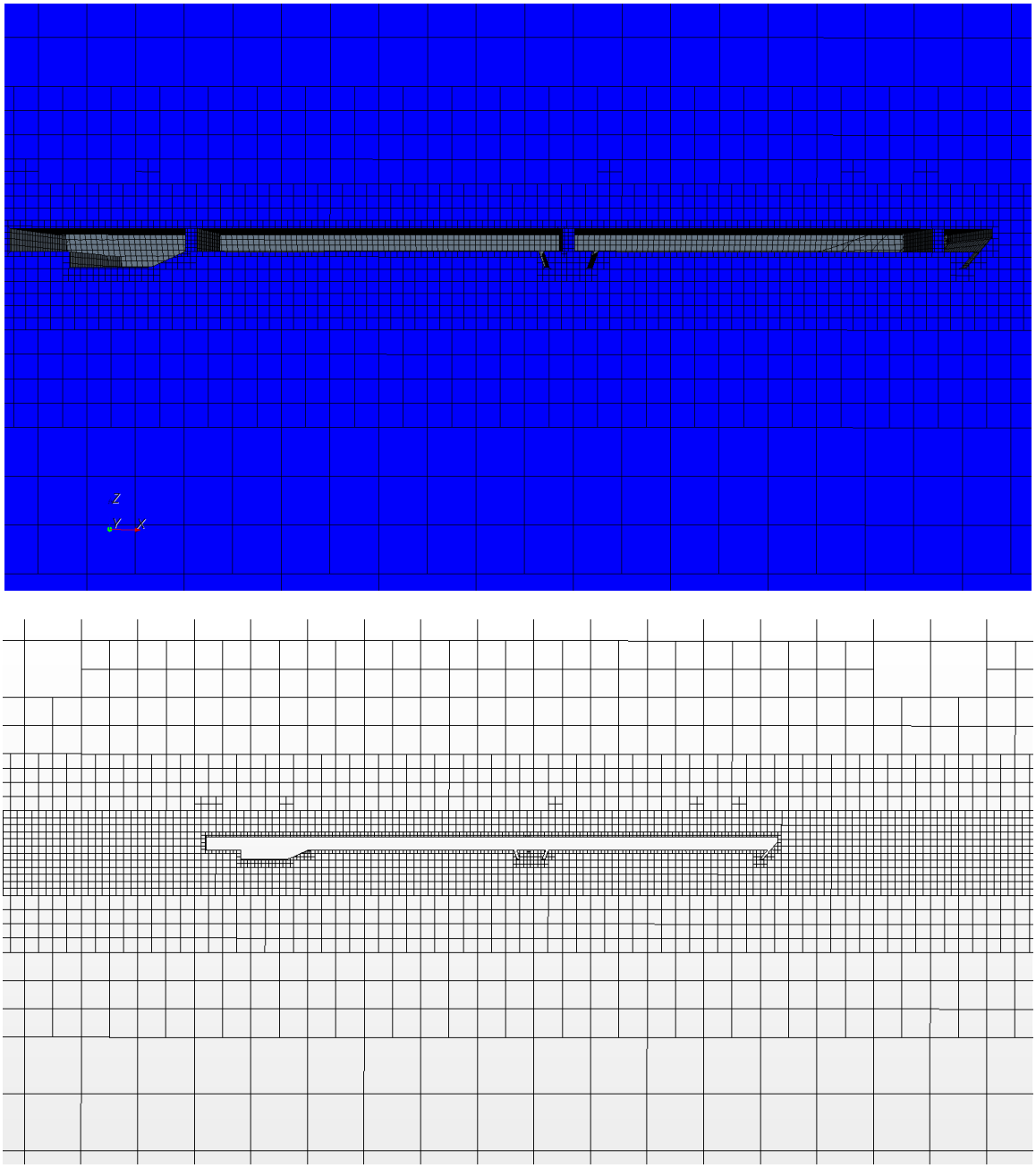

Figure 6: Coarse mesh symmetry plane.

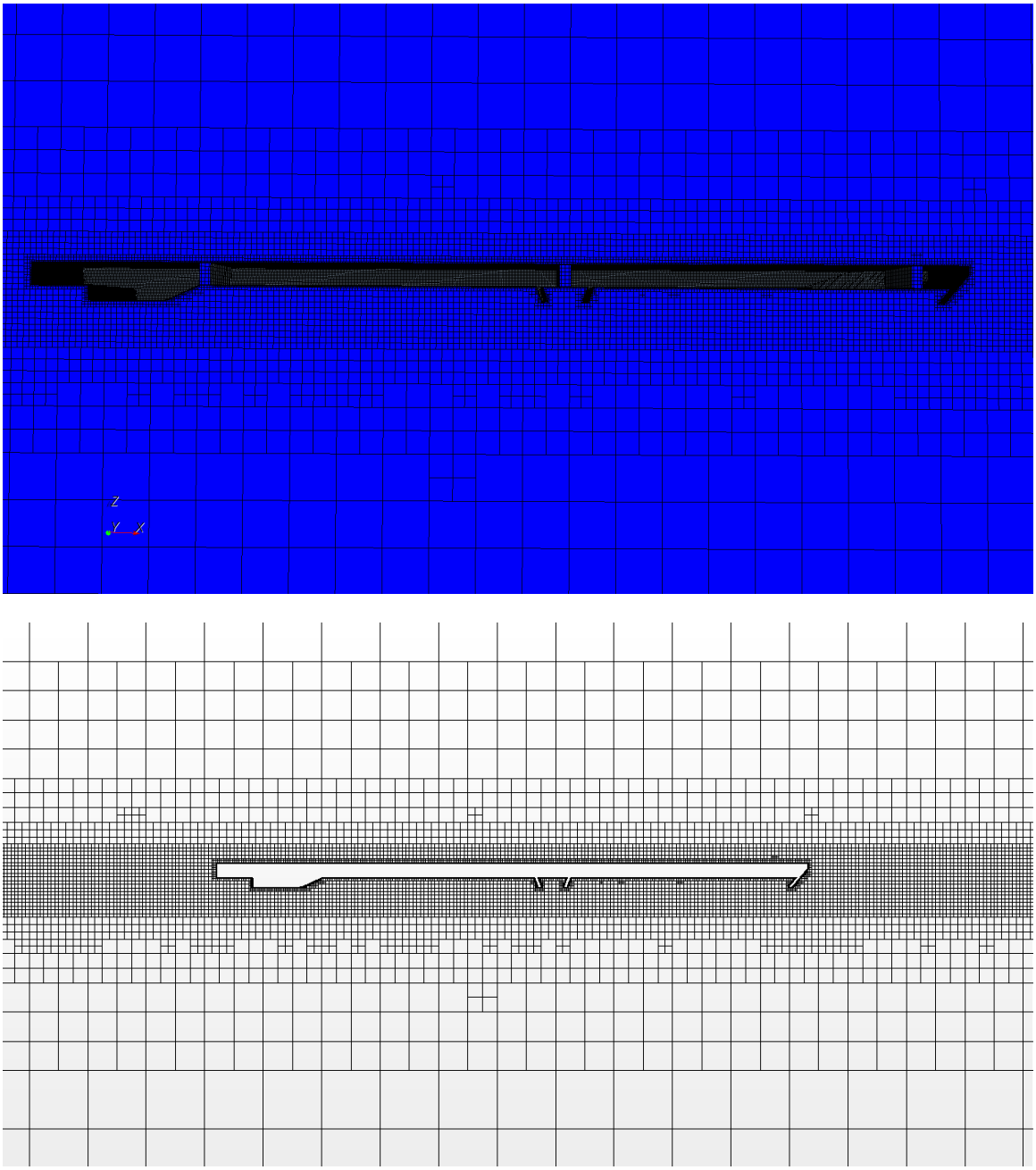

Figure 7: Fine mesh symmetry plane.

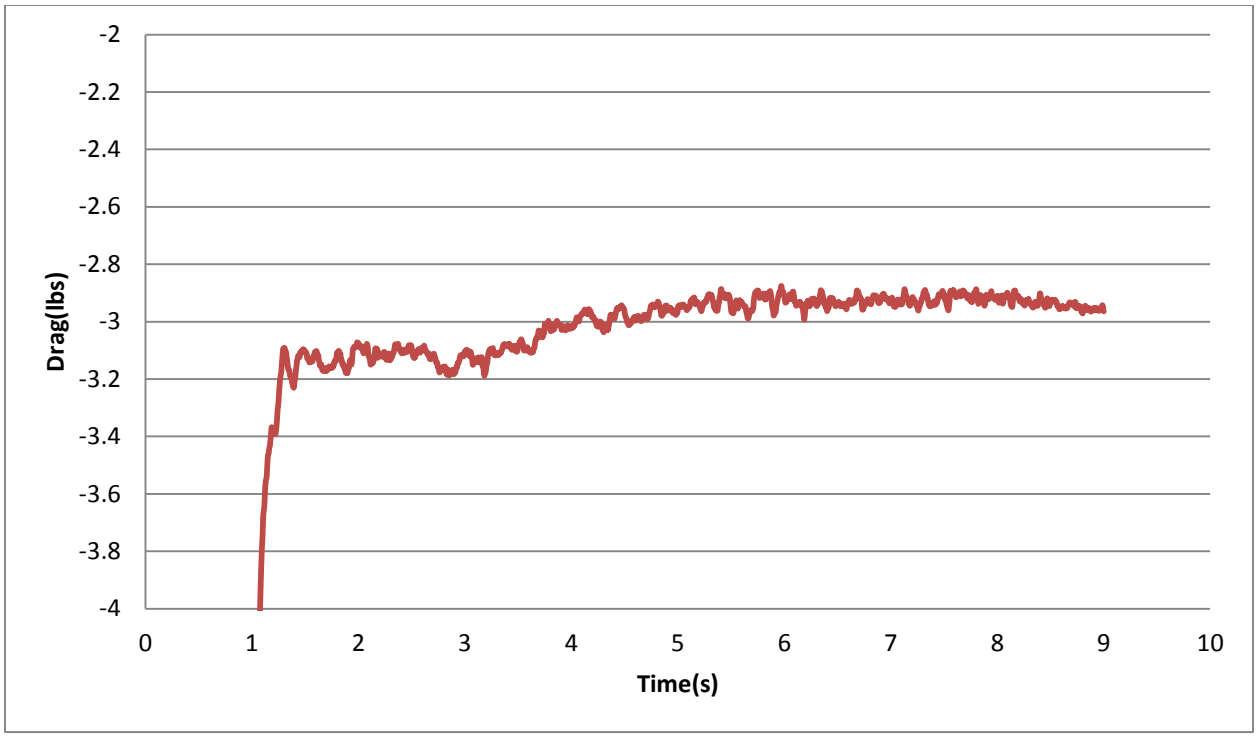

Figure 8: Time history of the drag on the half-model for the Fn 0.6 fine mesh inviscid simulation.

The converged inviscid drag for the half model at a Froude number of 0.6 can be seen above in can be seen above in Figure 8. Final drag values are averaged after four seconds of simulation time in order to allow time for the flow to develop around the body and become steady. It can be seen in Figure 9 that the drag values converge in an oscillatory manner as the mesh becomes more refined. The grid size is normalized by the finest mesh to generate the grid spacing, *h*. The grid refinement error estimation is derived from generalized Richardson extrapolation following Roache [8]. In order to perform a Richardson extrapolation error estimate the three finest meshes are considered so that the solution is converging monotonically.

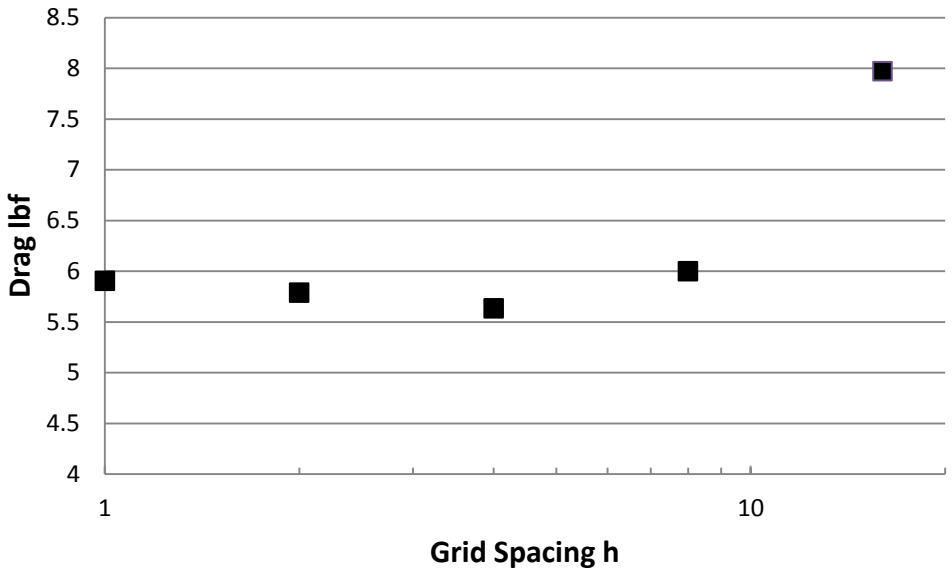

Figure 9: Fn 0.6 inviscid simulation averaged drag results compared to normalized grid spacing.

Changes between the fine/medium-fine, $\varepsilon_{k_{21}} = \hat{S}_{k_2} - \hat{S}_{k_1}$ and the medium-fine/medium $\varepsilon_{k_{32}} = \hat{S}_{k_3} - \hat{S}_{k_2}$ solutions are used to define the convergence ratio $R_k = \varepsilon_{k_{21}} / \varepsilon_{k_{32}}$ where $\hat{S}_{k_1}$, $\hat{S}_{k_2}$, and $\hat{S}_{k_3}$ correspond to the drag solutions on the fine, fine-medium, and medium grids, respectively. For uniform parameter refinement ratio, $r_k = \sqrt[4]{2}$, the estimates for error and order of accuracy can be calculated using the following equations

$$p_k = \frac{\ln\left(\varepsilon_{k_{32}} / \varepsilon_{k_{21}}\right)}{\ln\left(r_k\right)} \tag{3}$$

$$\delta^*_{RE_{k_1}} = \frac{\varepsilon_{k_{21}}}{r_k^{p_k} - 1} \tag{4}$$

The observed order of accuracy, p_k, is calculated to be approximately 2.16, which is only slightly higher than the formal order of accuracy of 2. The generalized relative error, $\delta^*_{RE_{k_1}}$, can then be calculated as approximately 4%. This relative error is small and it can be concluded that the finely meshed domain is adequately refined in order to provide reliable solutions. The fine mesh was used for all subsequent simulations. During these simulations at a Froude number of 0.6 other characteristics were monitored as well, including heave and pitch motions, to ensure the results were as expected. The free surface elevation and wake profile can be seen in Figure 10 showing the free surface around the hull and underneath the cushion. In this way an adequate mesh resolution was determined.

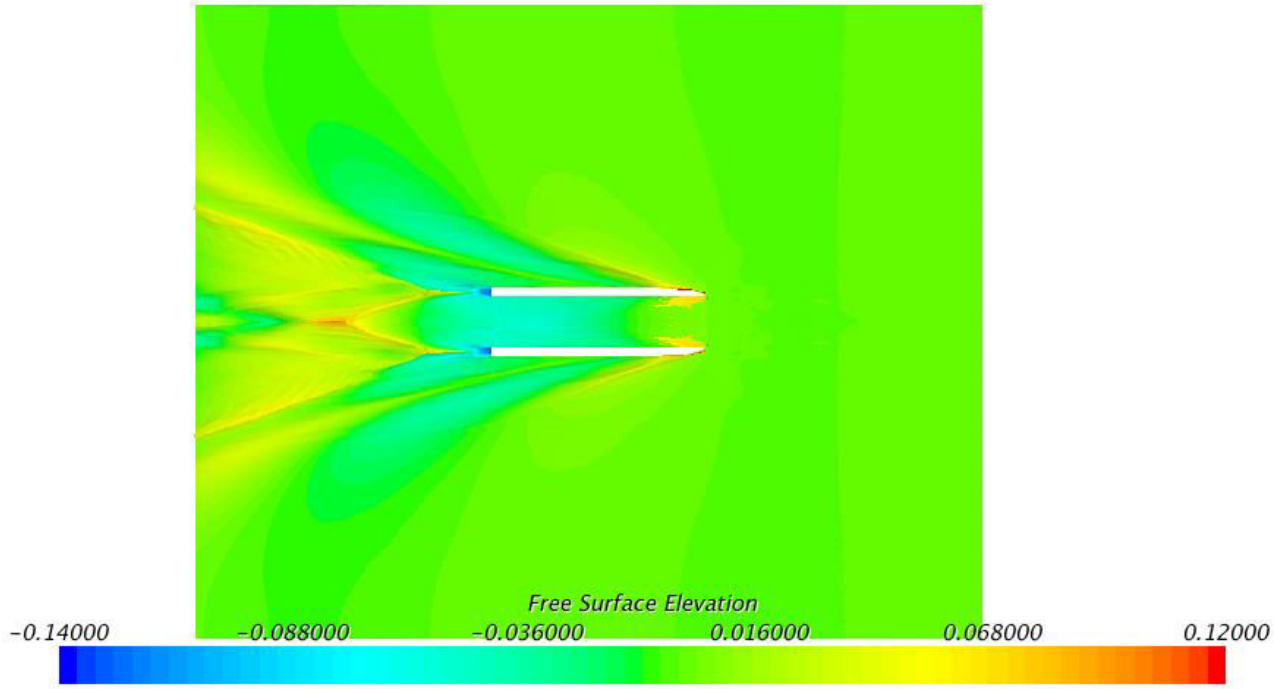

Figure 10: Fn 0.6 inviscid simulation wake profile from fine mesh solution.

4.1 Verification and Validation Consideration

The process of verification and validation attempts to assess accuracy and reliability within CFD simulations. Verification and validation is incredibly important when working with numerical simulations and a comprehensive suite of information can be found in Roache [9], Oberkampf [10], and Veluri [11], and their additional references. Verification is the assessment of the accuracy of the solution to a computational model by comparison with known solutions. Validation is the assessment of the accuracy of a computational simulation by comparison with experimental data. In this manner verification seeks to identify code errors and validation seeks to identify theory errors. While verification and validation for CFD problems is extremely important it is a far reaching topic and outside the scope of the work offered here. However, it is important to note that the grid refinement study presented is a method of solution verification. Through this solution verification it was shown that the behavior of the solution matches the formal rate of convergence for the numerical scheme. Additional verification and validation work involving the CFD code STAR-CCM+ and relating to multiple aspects of the surface effect ship problem was presented by Bloxom [4].

5. Viscous Simulations

In order to model a realistic situation, the effects of turbulence were added to the simulation. The turbulence model Spalart-Allmaras involves solving a single transport equation to determine the turbulent viscosity. The primary goal of implementing these viscous simulations was to more accurately replicate the model tests. However, it was also important to determine the effect of the rigid seals and how the drag, pitch, and heave of the craft differ from the inviscid simulations. In order to accurately resolve the turbulent boundary layer a very small prism layer was added all around the SES body. The added prism layer mesh can be seen below in Figure 11.

The drag results were broken down into components which include both the shear and pressure drag caused by both the air and water. These drag components were monitored for the hull as well as for all three seals. The major drag components and total drag for the half model can be seen in Figure 12. The drag due to the water on each seal is minimal ensuring a small gap between the seal and the free surface. The majority of the seal drag is due to the pressure drag from the air cushion. The majority of the drag on the hull is composed of the water shear and pressure drag. The water shear drag makes up a large portion of the total drag and shows how not calculating the shear drag in inviscid simulations can be a large source of error.

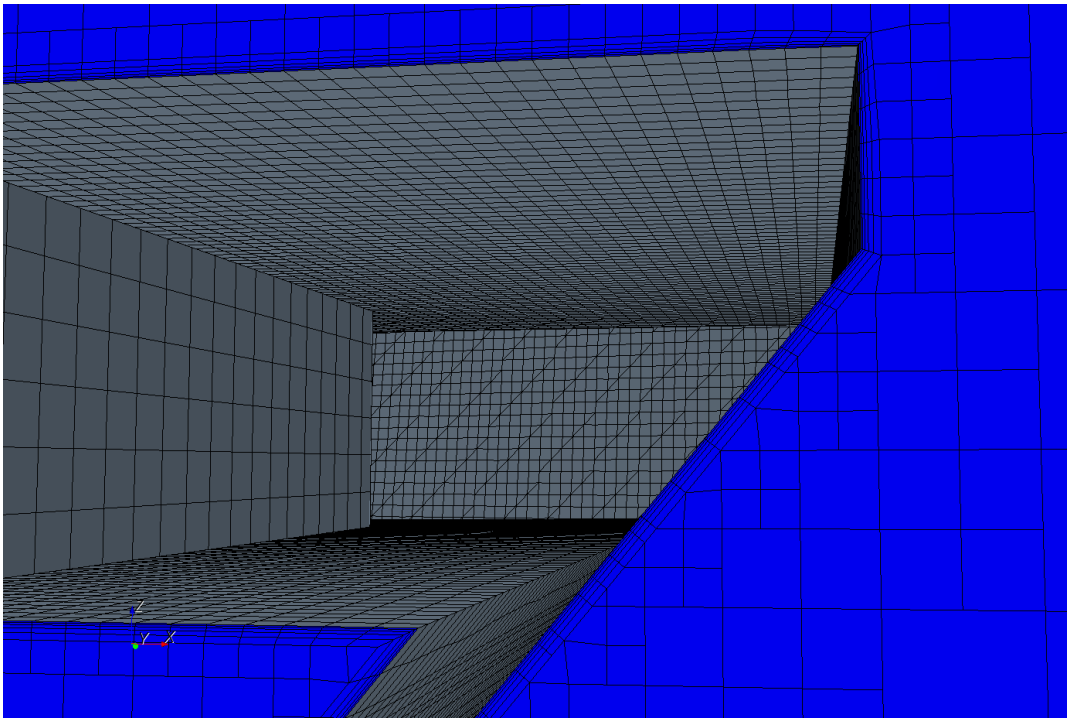

Figure 11: Prism layer mesh for viscous simulations.

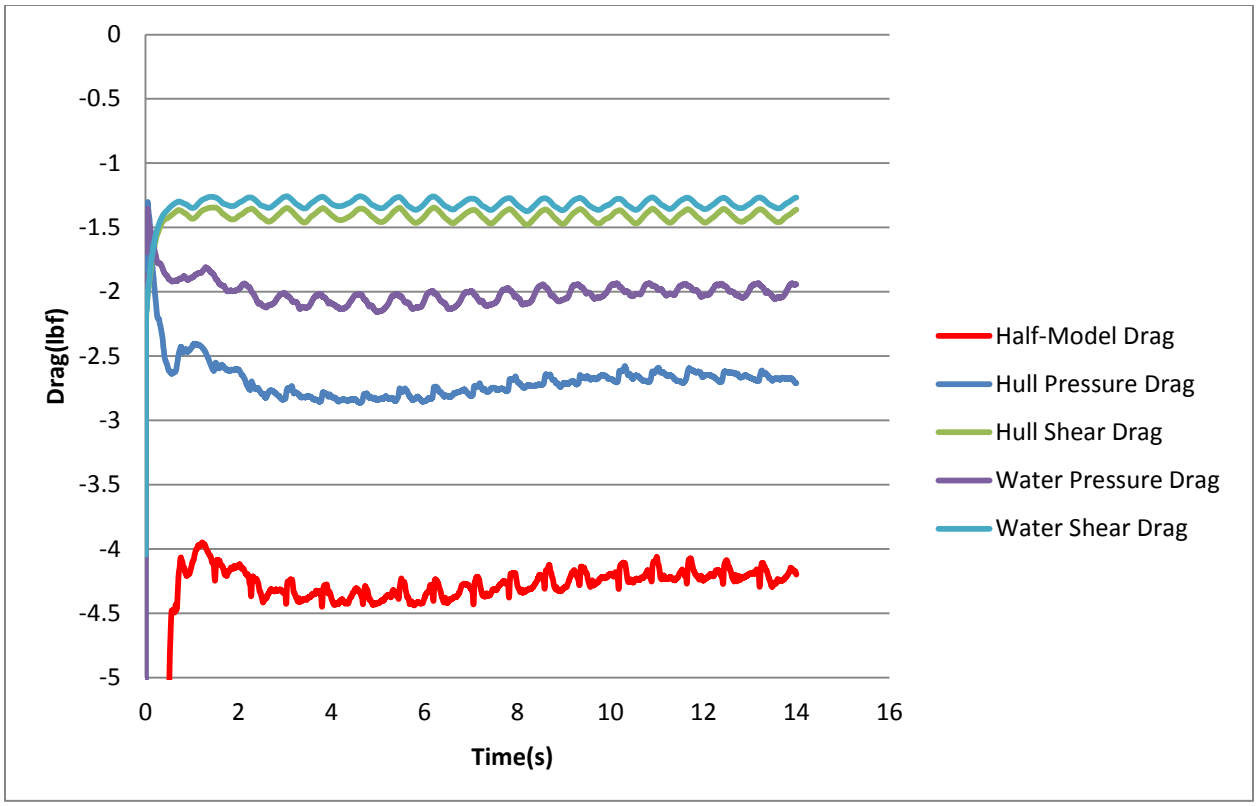

Figure 12: Time history of the major drag components on the half-model for the Fn 0.6 viscous simulation.

An important issue arises when comparing the drag results for the inviscid and viscous simulations. Both drag results have some noise and fluctuation in them that must be averaged out. The viscous simulations drag, however, appear to have some oscillatory nature to them. The heave and pitch motions of the SES were then examined to determine where the drag oscillations stem from. The heave motions are of very small magnitudes during these calm water simulations. The pitch motions for the viscous simulation can be seen in Figure 13. When looking at the pitch plot it can be seen that the SES pitches in an oscillatory manner through a range of four-tenths of a degree. In comparison to the inviscid pitching of the SES it can be seen that no oscillatory motion is present as seen in Figure 14. The introduction of viscosity has caused an increased drag on the SES seals and excited a pitching motion on the body.

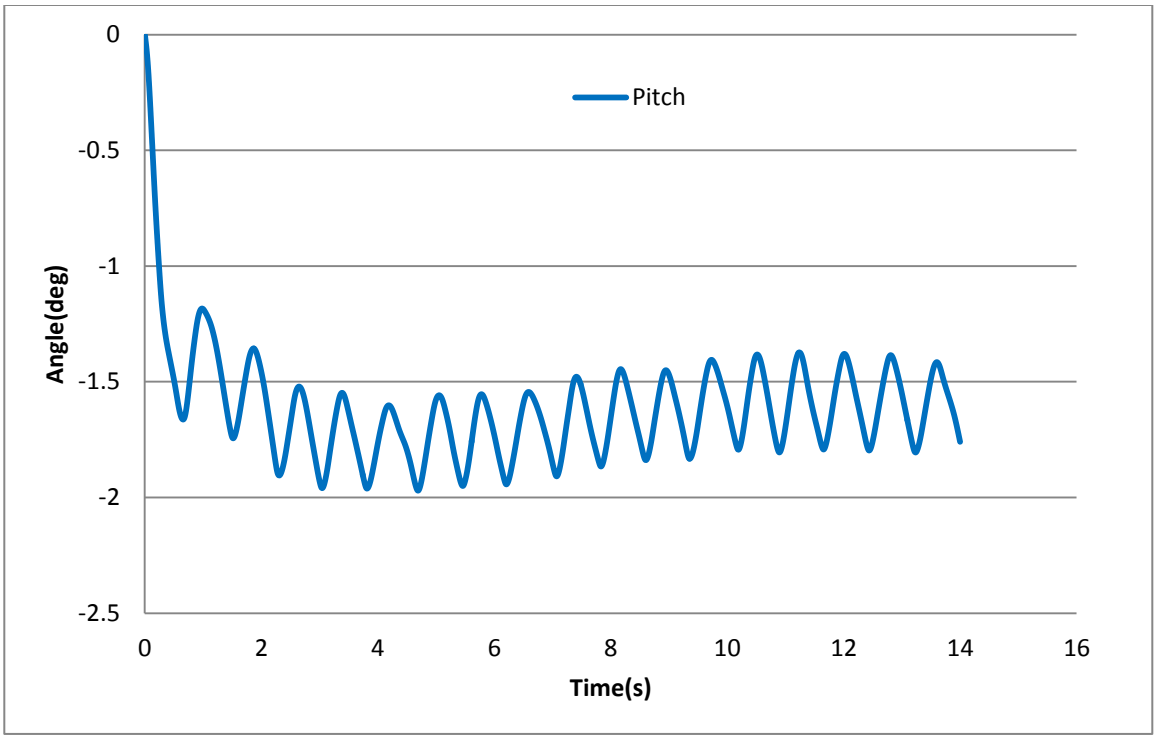

Figure 13: Time history of the pitch for the Fn 0.6 viscous simulation.

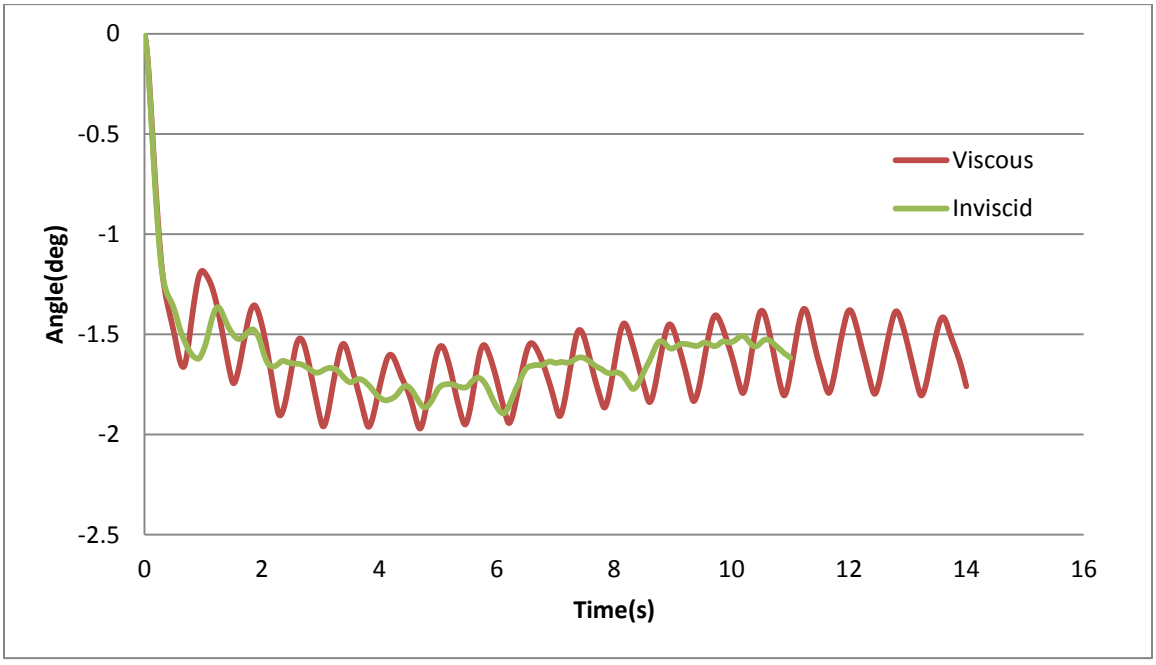

Figure 14: Time history of the SES pitch for the Fn 0.6 viscous and inviscid simulations.

For the viscous drag this oscillation in pitch seems to be what causes the oscillations in drag. Below in Figure 15 the drag and pitch for the viscous simulation at Fn 0.6 have been plotted on the same graph for comparison. The heave values are so small in magnitude that they seem to be unimportant. However, when investigating the pitch and drag a pattern can be seen.

Spikes in drag correspond to the SES pitching bow up. This bow up position would cause an increased drag on the large aft seal. The large aft seal has a lot of surface area that could possibly interact with the free surface. With the addition of shear drag acting on the aft seal the spikes in drag could be accounted for. The addition of viscous shear drags on the hull, and more importantly the skirts, have induced small oscillations in pitch and drag. However, these small fluctuations can be averaged out to determine final drag values. So when determining an average drag it is important to take values after the simulation has reached a quasi-steady state and in an integer number of periods. The pitch orientation can be seen below in the volume fraction of air representation, Figure 16, and the wake profile can be seen in Figure 17.

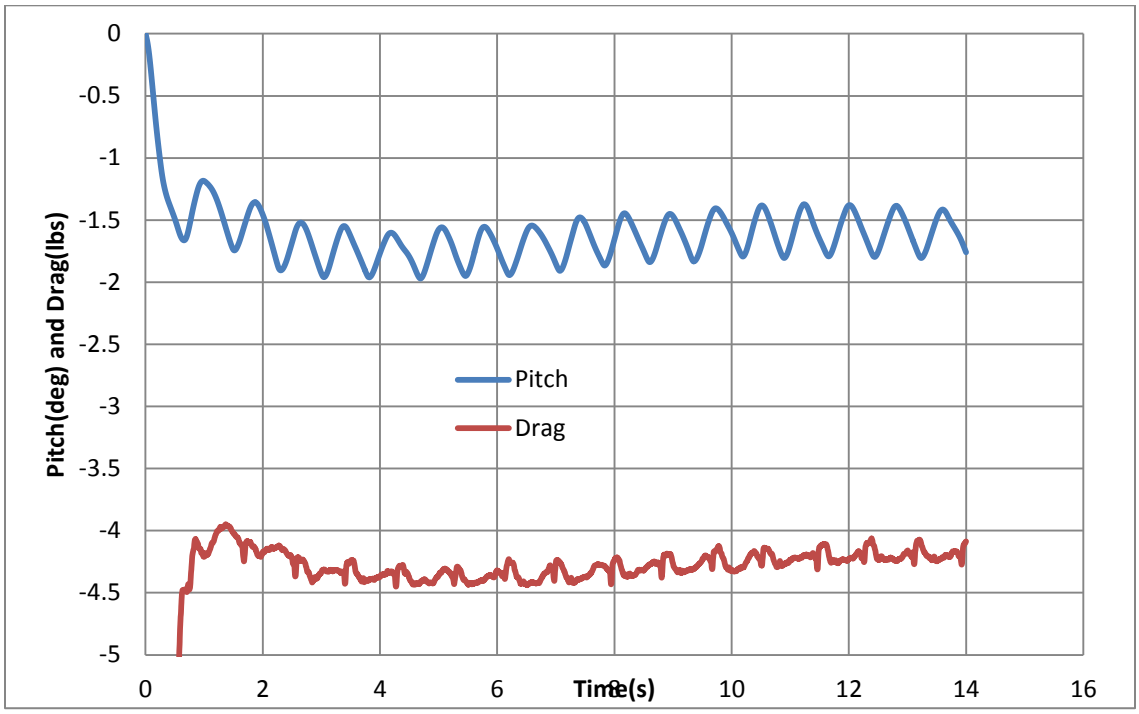

Figure 15: Time history of the drag and pitch for the Fn 0.6 viscous simulation.

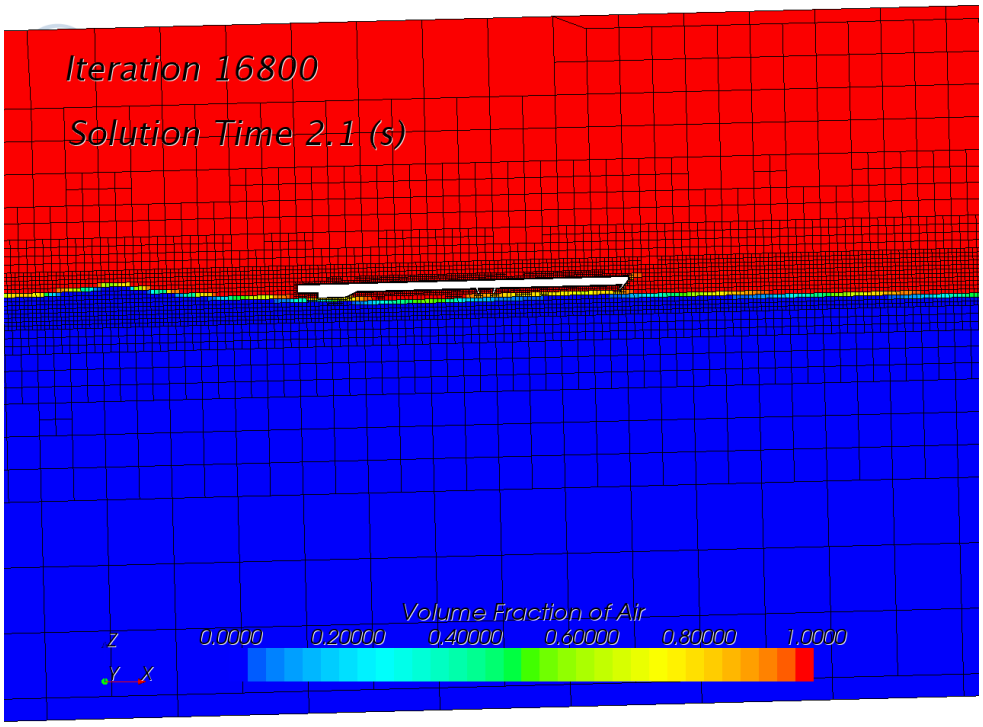

Figure 16: SES Fn 0.6 viscous simulation volume fraction of air.

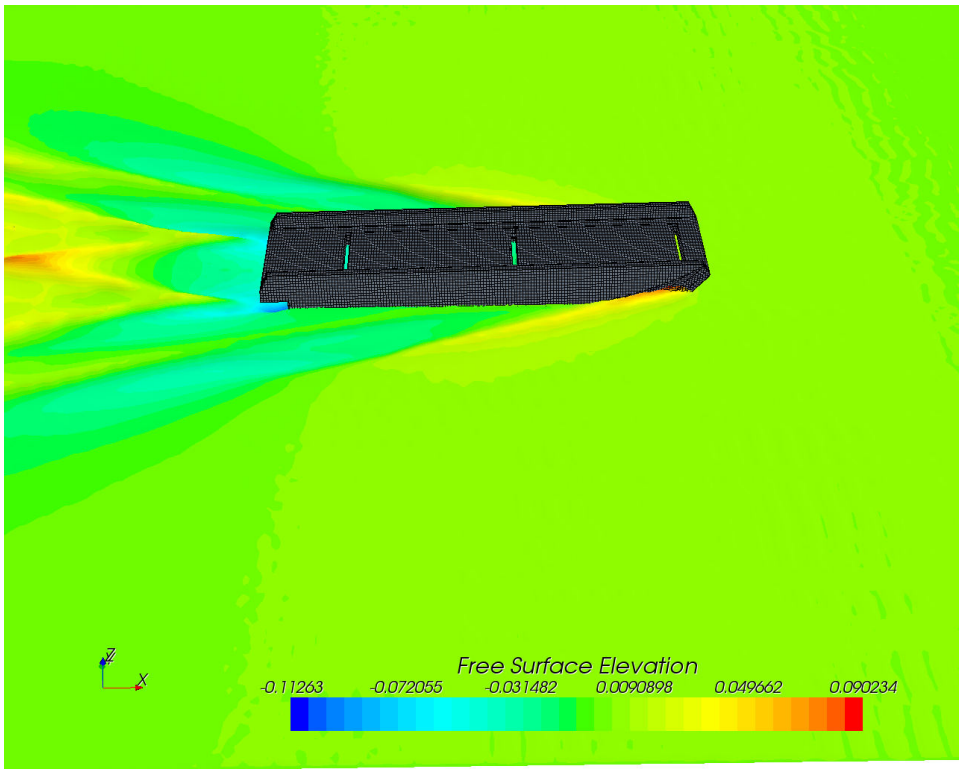

Figure 17: Free surface contours for the Fn 0.6 viscous simulation.

Comparisons of the free surface contours for the viscous and inviscid simulations at Froude number of 0.6 can be seen in Figure 18. They are very similar with comparable flow features and wake patterns. The bow wave from the inviscid simulation is slightly larger, while the rear wake in the viscous simulation may be higher.

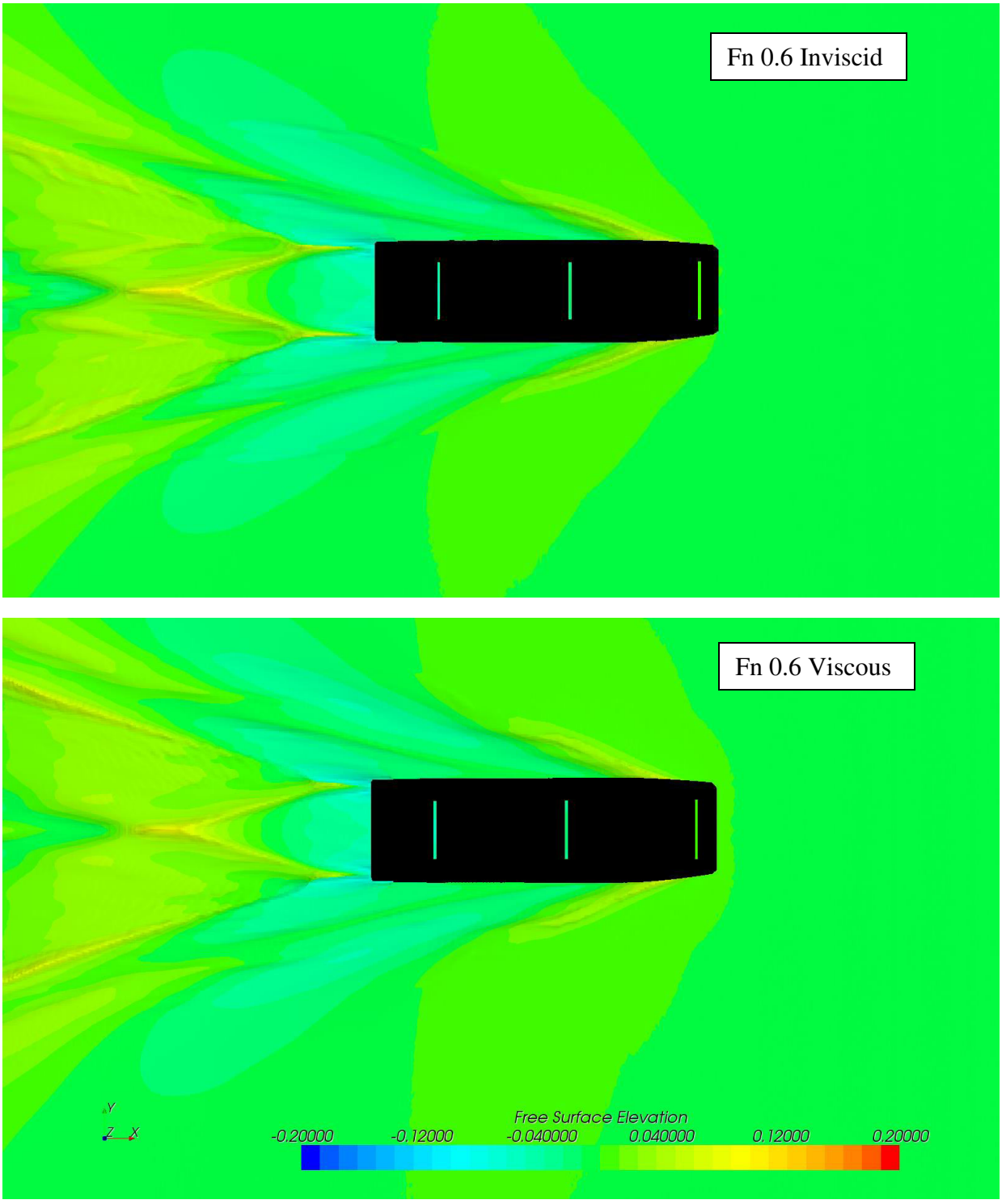

Figure 18: Free surface contours for the Fn 0.6 inviscid and viscous simulations.

5.1 Analytical and Numerical Comparison

The drag results for the numerical simulations and the model test are compared in Figure 19. For the purposes of the research presented here, when comparing experimental and numerical drag results, time accuracy is not considered, only the quasi-steady state drag values are compared. It can be seen that the inviscid simulation full model drag results significantly under predict the experimental drag results. This leads to the conclusion that viscosity modeling is necessary in order to achieve results that are closer to the model test results. However, the viscous simulation overestimates the drag results of the experimental data. This is most likely due to the rigid skirt approximation which causes a significant increase in drag as the rigid skirts interact with the free surface. Further investigation of the effect of the rigid skirt approximation will be discussed below as well as possible solutions to the issue. Additional comparison of numerical simulations with experimental data of free surface flow about a surface effect ship can be found in Donnelly [12].

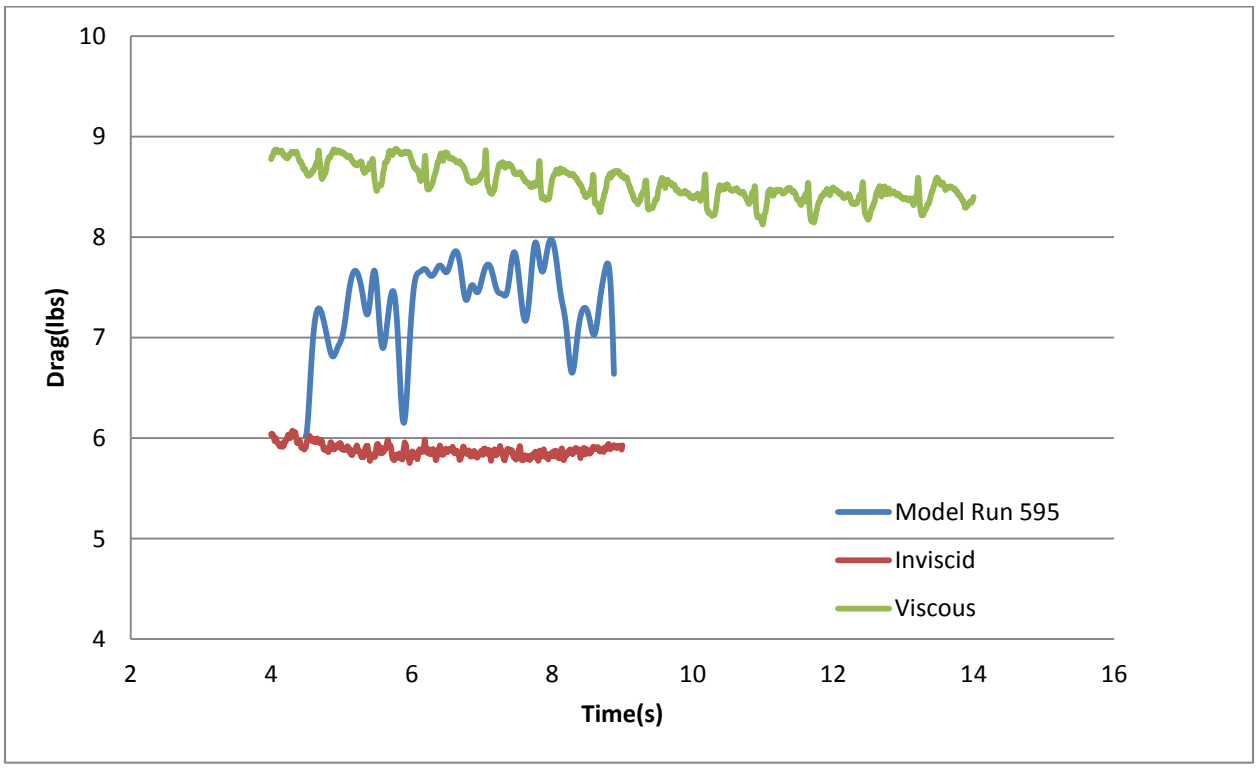

Figure 19: Comparison of the Fn 0.6 experimental run, inviscid simulation, and viscous simulation full model total drag results.

6. Numerical Simulation of Wave Cases

While numerical simulations of calm water cases have been shown to produce desirable results for SES simulations, running an SES simulation in wave cases has yet to be accomplished within STAR-CCM+. A CFD simulation of a SES in waves is a very challenging problem, as discussed in Lin et al [13] and Kring et al [14], which requires careful consideration. Some numerical simulation work involving a SES in waves has been accomplished but significant

errors still exist, Bhusan et al [15]. Comparisons of experimental test data for the SES model with numerical simulation data in a multitude of wave cases is the final objective. However, simulations involving a surface effect ship in waves is complex and preceding SES simulations in waves, the capabilities of STAR-CCM+ to model wave cases needs to be investigated.

A VOF Waves model can be used to simulate surface gravity waves on the fluid interface. The waves generated are fully three dimensional and have myriad ways of being modeled. The wave models available include a simple first order wave approximation to Stokes wave theory. This model generates a regular, periodic sinusoidal wave where velocity, amplitude, and wave length or wave period can be specified. Also in this model a deep water dispersion relation approximation can be applied. Similarly a fifth order approximation to Stokes theory of waves can be used. This wave more closely resembles a real wave than one generated using the first order method. The wave profile and phase velocity depend on wave height, current velocity, and water depth which must be specified. A generic work boat hull form was run in head seas using the fifth order wave approximation. The heave and pitch were monitored and can be seen in Figure 20 and Figure 21 below. The hull form interacting with the surface waves can be seen in Figure 22.

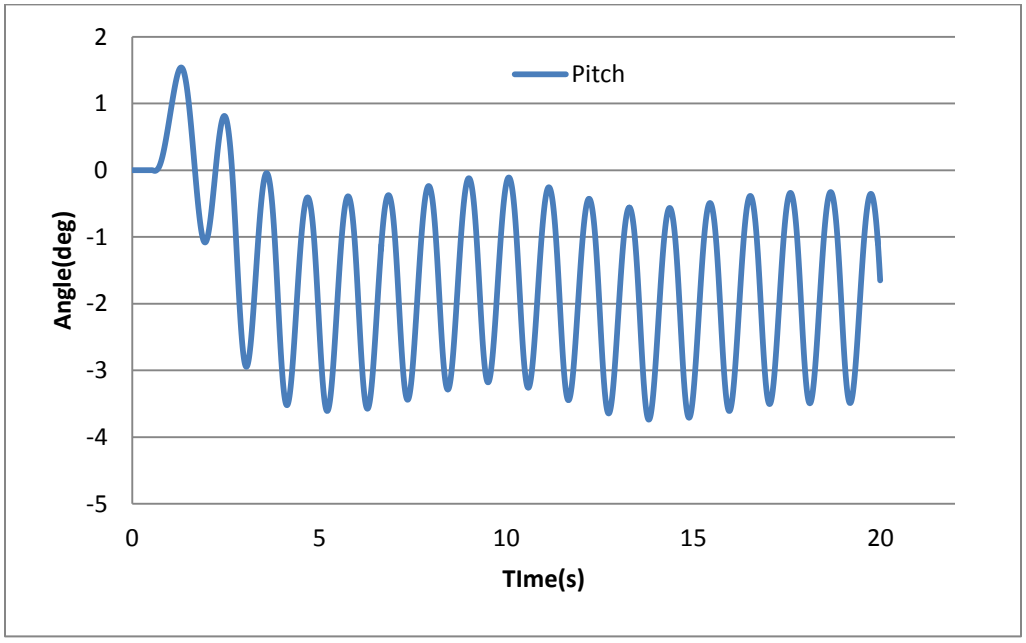

Figure 20: Generic hull form pitch time history in regular waves.

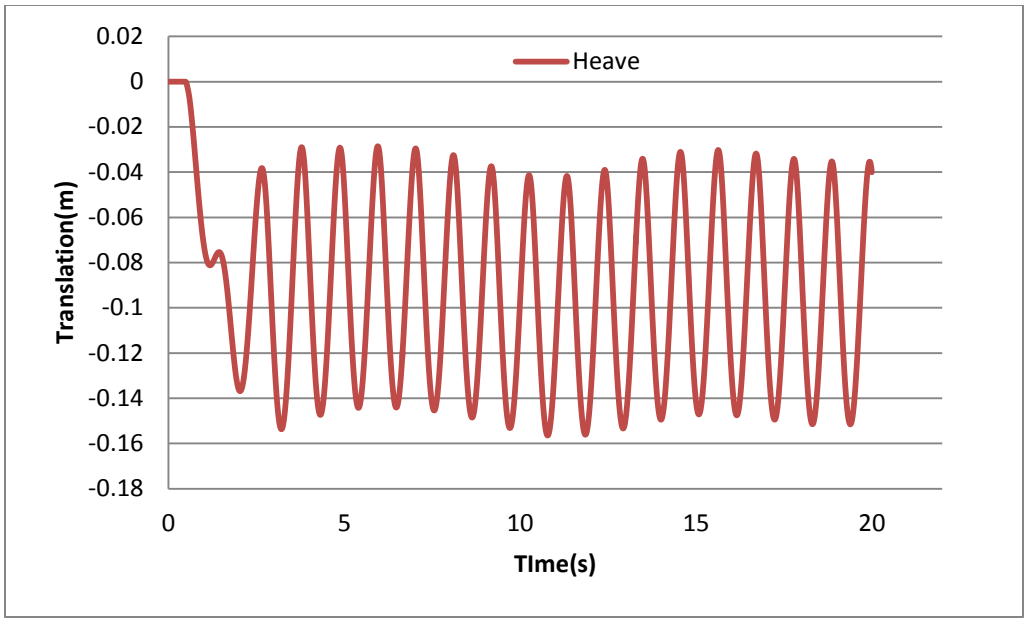

Figure 21: Generic hull form heave time history in regular waves.

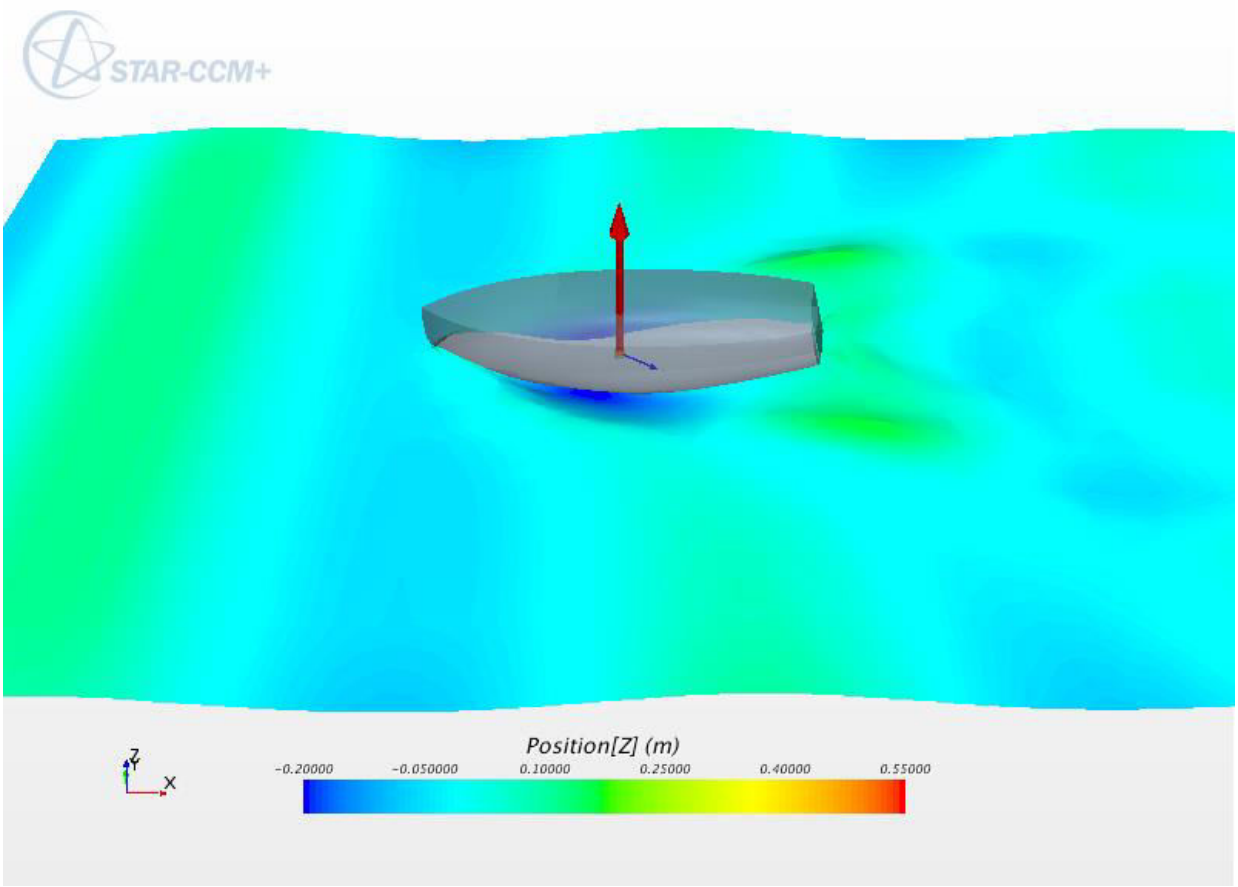

Figure 22: Generic hull form wave profile in regular waves.

STAR-CCM+ also has the capabilities to model more complex wave phenomena. A series of first order waves can be used to create a complex seaway. A superposition wave uses a linear superposition of different sinusoidal waves to simulate more irregular seas such as a cross sea or spectral waves. Finally, an irregular wave can be used to describe a short-term sea state by a wave spectrum, which is the power spectral density function of the vertical sea surface displacement. The significant wave height and peak wave period are specified, and the Pierson-Moskowitz spectrum is used to model the irregular seaway. The Pierson-Moskowitz spectrum is used for fully developed seas only. However, the JONSWAP spectrum can also be included to extend the Pierson-Moskowitz spectrum to describe developing sea states and fetch limited seas. The JONSWAP specification allows for the specification of peak shapes and spectral widths for the irregular wave. The same work boat hull form was run in a simulation for irregular head seas using the Pierson-Moskowitz spectrum. The pitch and heave were monitored and can be seen in Figure 23 and Figure 24. As well the wave profile can be seen below in Figure 25.

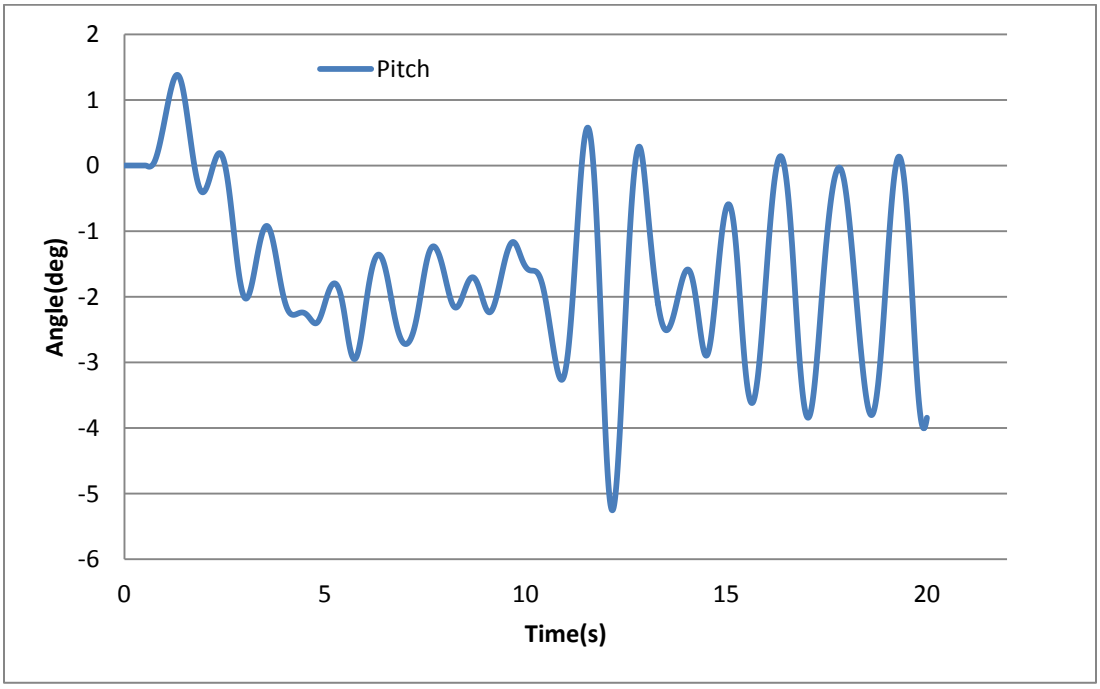

Figure 23: Generic hull form pitch time history in irregular waves.

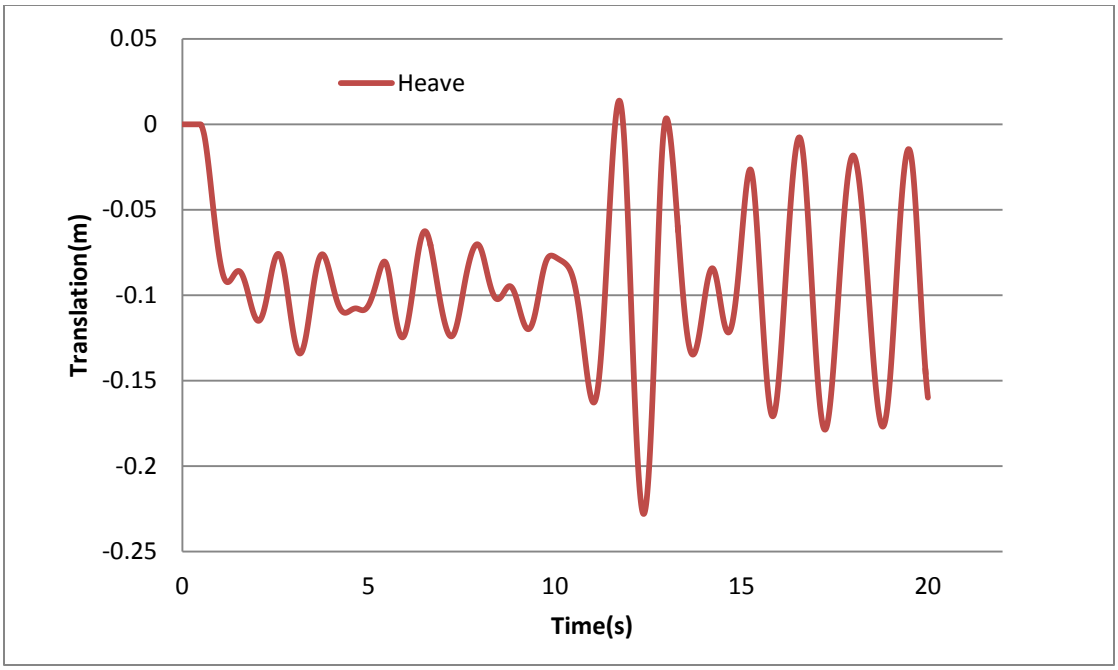

Figure 24: Generic hull form heave time history in irregular waves.

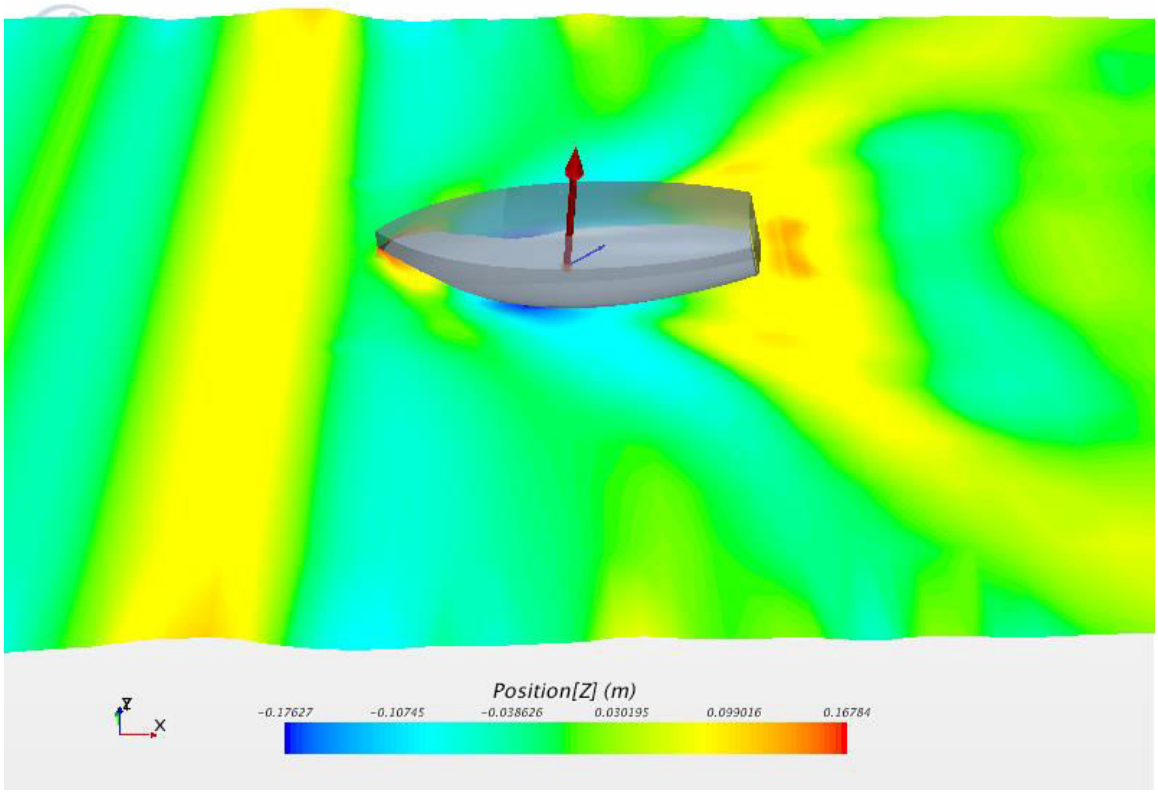

Figure 25: Generic hull form wave profile in irregular waves.

The pitch and heave seen for the regular fifth order wave case have very defined periodic oscillations. The pitch and heave reach a generally steady state with only small variations in amplitude, which would be expected due to the time dependency of the simulation. The sinusoidal motions as the vessel encounters the regular waves is then compared the motions of the vessel in irregular seas. It can be seen that the pitch and heave have irregular and random oscillations and the boat encounters the irregular waves generated by using the Pierson-Moskowitz energy density spectrum. After successful simulations of the simple hull form in differing wave cases, the next step is to simulate the SES craft in waves.

7. Skirt Approximation Issues

The dynamic flexible skirts of the SES model are currently simplified in the numerical simulation. The skirts have been modeled as flat geometries as opposed to finger or lobe type seals. As well the skirts have been approximated as rigid and shortened to the natural waterline. As seen during simulations the rigid skirts interact with the free surface causing drastically unrealistic drag calculations. The plowing effect of rigid skirts can be seen for the original full length skirts in Figure 26 as the rigid seals interact with the free surface. Similar situations would occur when running the current SES configuration in waves. As well, the gap underneath the shortened skirts causes unrealistic air leakage which can be seen in Figure 27 where velocity vectors can be seen underneath the skirt on the surface. This jet air leakage can cause unwanted oscillations as the momentum sources attempt to maintain the interior cushion pressure.

Figure 26: Rigid skirts interacting with free surface, Donnelly [16].

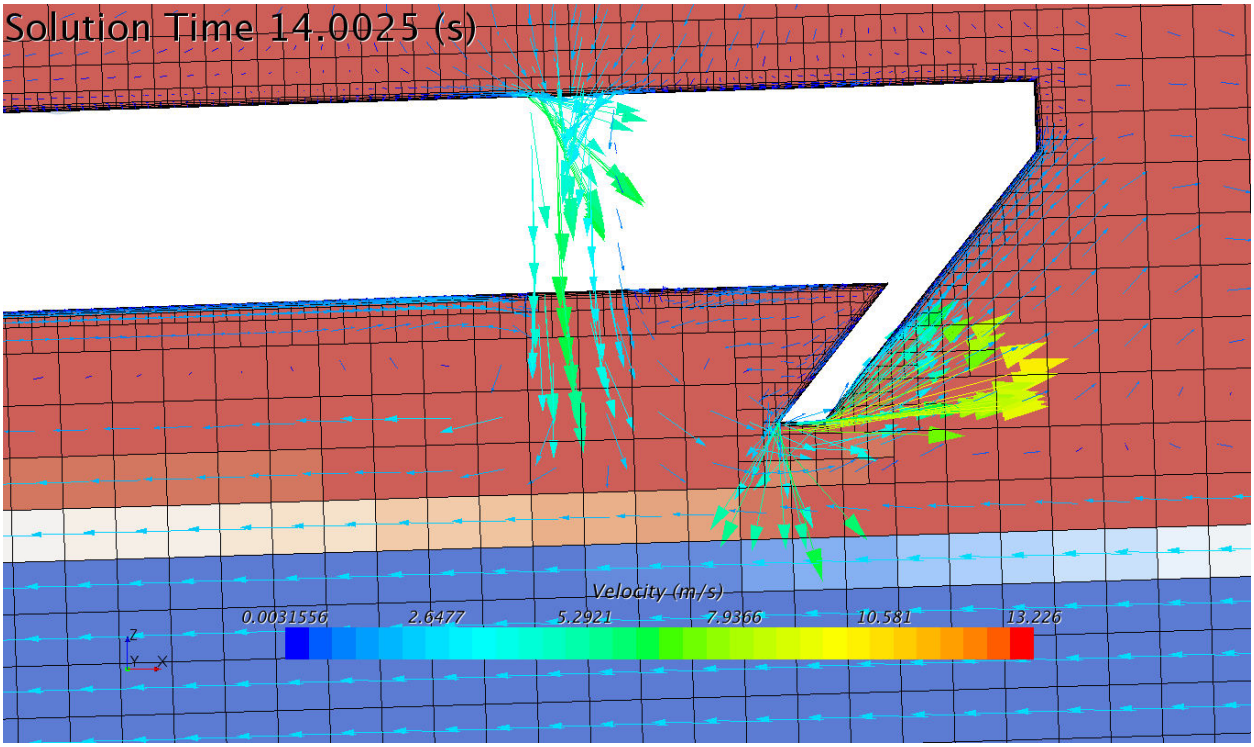

Figure 27: Air cushion leakage.

Therefore, in order to properly model the SES in calm water and in wave case simulations the dynamic, flexible skirts must be modeled correctly. Current research in the field of fluid-structure interaction (FSI) would allow for numerical simulations of these flexible skirts to take place. FSI problems involve coupling of fluid dynamics and structural analysis. An iterative process passes information back and forth during a co-simulation in order to resolve the fluid flow and structural response. A co-simulation involving STAR-CCM+ and the structural finite element code Abaqus FEA has been be used to model the flexible dynamic skirts of a SES. Work performed by Bloxom [4] investigates FSI problems for SES bow seals, and in Figure 28 a simplified simulation can be seen in which only the front skirt is being modeled. Current technological limitations mean that FSI problems are very difficult and computationally expensive. A numerical simulation involving the full surface effect ship model would require finite element analysis of three different skirts. As well the skirt geometry would need to be modeled correctly as finger or lobe seals to accurately represent the SES model. Therefore, a SES numerical simulation with fully dynamic and flexible seals is a very costly and difficult problem that is still elusive.

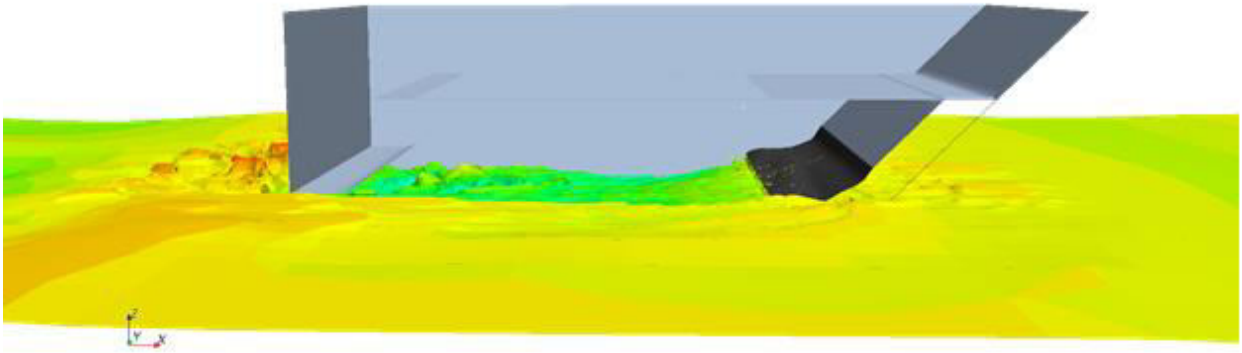

Figure 28: FSI Simulation of Flexible Seal, Bloxom [4].

8. Porous Skirt Modeling

In an attempt to solve the current problem of modeling the SES skirts, an alternative method was developed. The primary use of skirts on an air cushion vehicle is to trap air in a high pressure region underneath the craft. The idea behind this alternative method is to create a skirt that would still be rigid, but would not interact with the free surface. This would allow for the cushion pressure to be maintained while not increasing the drag due to the seal interacting with the free surface. As well, the skirt would prevent jet leakage gaps which can induce unwanted oscillatory motions. This could be accomplished by modeling the skirts as infinitesimal thickness flat plates incorporating a porosity function. The desired effect would be to model a skirt that prevents the flow of air while allowing the free flow of water.

The porosity function implemented calculates the velocity across the porous boundary from the known pressure drop as follows in Equation 5 according to STAR-CMM+[17].

$$\Delta p = -\rho(\alpha|v_n|+\beta)\, v_n \tag{5}$$

Where v_n is the normal velocity across the porous boundary, α is the user-specified constant porous inertial resistance, β is the user-specified constant porous viscous resistance, and ρ is the fluid density at the interface. It is assumed that the direction of the flow is unchanged as is passes through the baffle. In order to specify porous resistance values differently for the water and air phases a user defined function was developed, where α is specified as zero while β is defined by the user function. The constant β is specified as zero for a cell with volume fraction of air less than 0.5 while β is specified as a linear increase from 0 to 10,000 for a volume fraction of air between 0.5 and 1. This specification allows for the free flow of water and blocks the flow of air without the rigid skirt interacting with the free surface. A simple test case of a porous skirt in

open water can be seen in Figure 29. As desired the flow through the bottom half of the skirt in water is undisturbed. Inversely, the upper portion of the skirt redirects the airflow around the plate. In the figure above velocity vectors can be seen along with porous resistance values. Next the same simple skirt is run in wave cases to ensure the model is working properly. Through monitoring the free surfaces velocities and pressure throughout the domain it can be seen that the wave passes through the porous skirt without any change in the flow field while the skirt is still impassable by the air phase. The porous skirt in waves can be seen below in Figure 30. This simplistic simulation involving and a single skirt in an open water wave condition leads to the possibility of modeling a full SES in wave conditions.

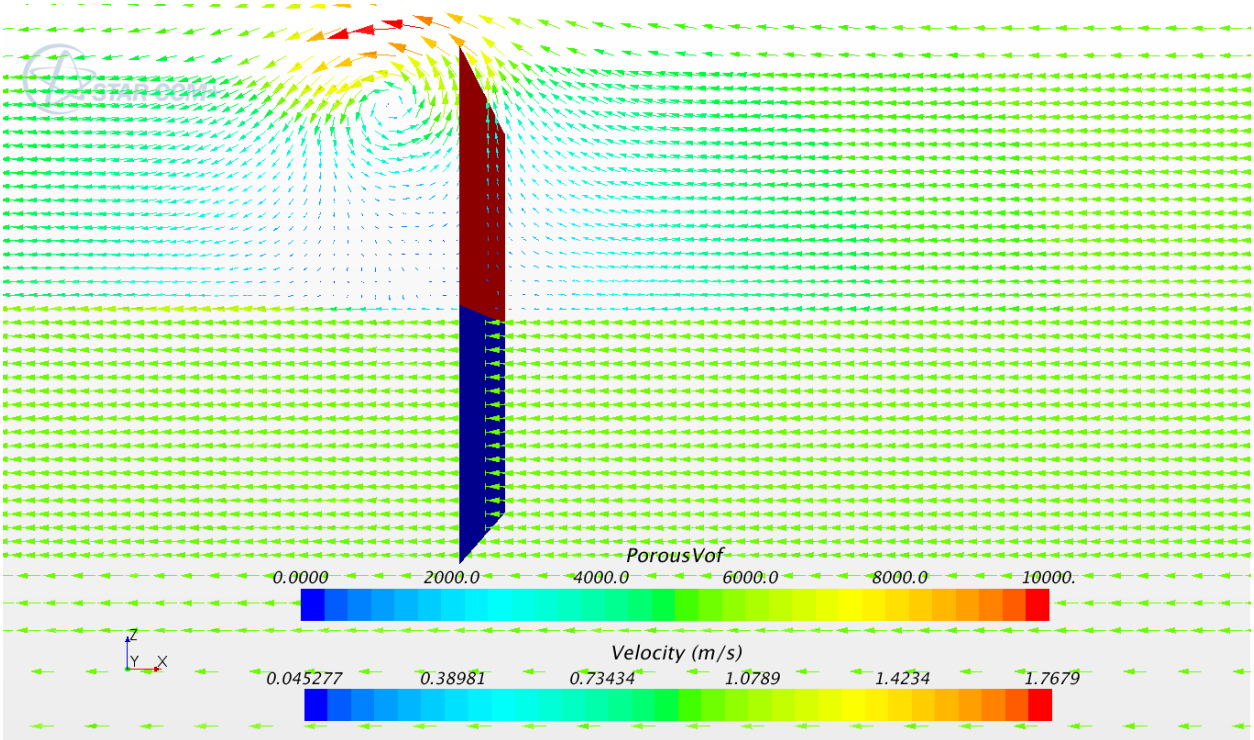

Figure 29: Open water porous skirt.

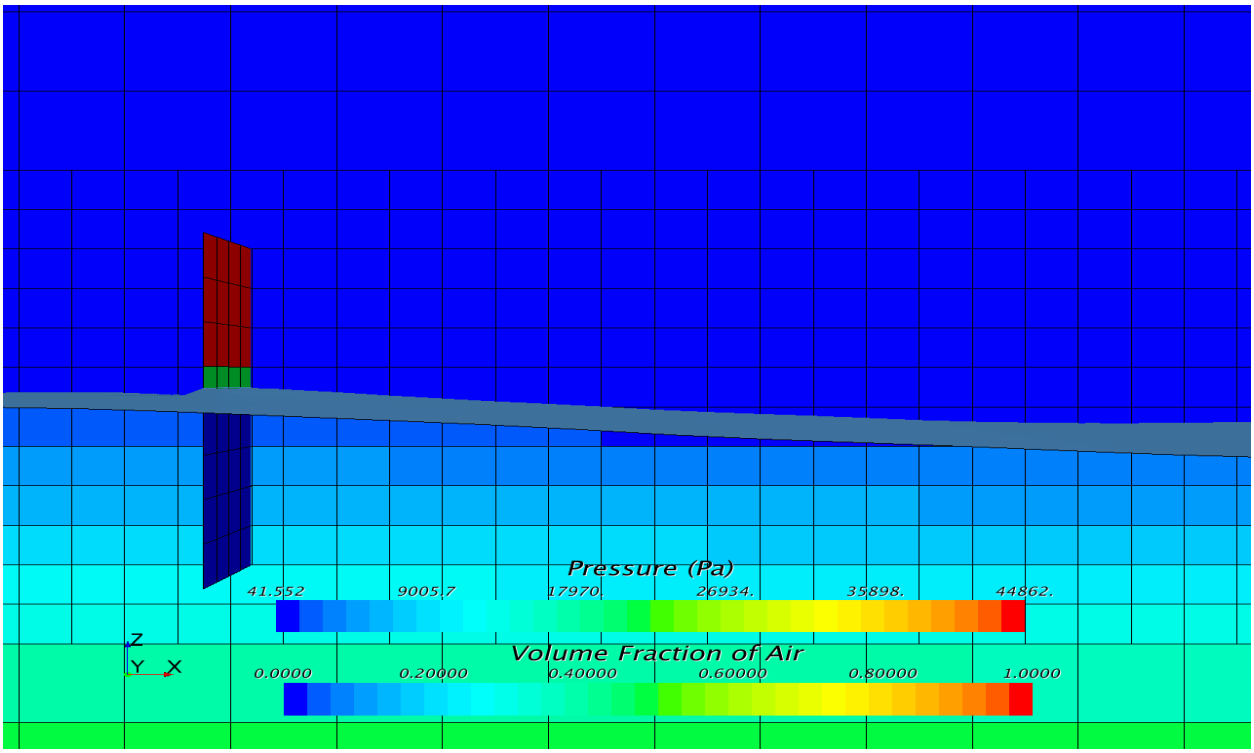

Figure 30: Porous skirt in waves.

8.1 SES Porous Skirt Implementation

It is hypothesized that this porosity model will allow for more accurate numerical simulations of the SES in calm water and the implementation of wave cases by comparison to the rigid seal approach. The cushion pressure will be trapped by the skirt, maintaining the SES functionality. However, the skirts will not interact with the free surface but instead allow for the wave to pass underneath the craft. The first step is to alter the geometry of the SES by implementing the infinitesimal thickness porous skirts. The new geometry can be seen in Figure 31 and the mesh can be seen in Figure 32. The skirts are returned to their full length according to the SES model design specifics. The mesh size determined by the grid convergence study was maintained during these simulations as well in order to accurately resolve the fluid flow about the SES.

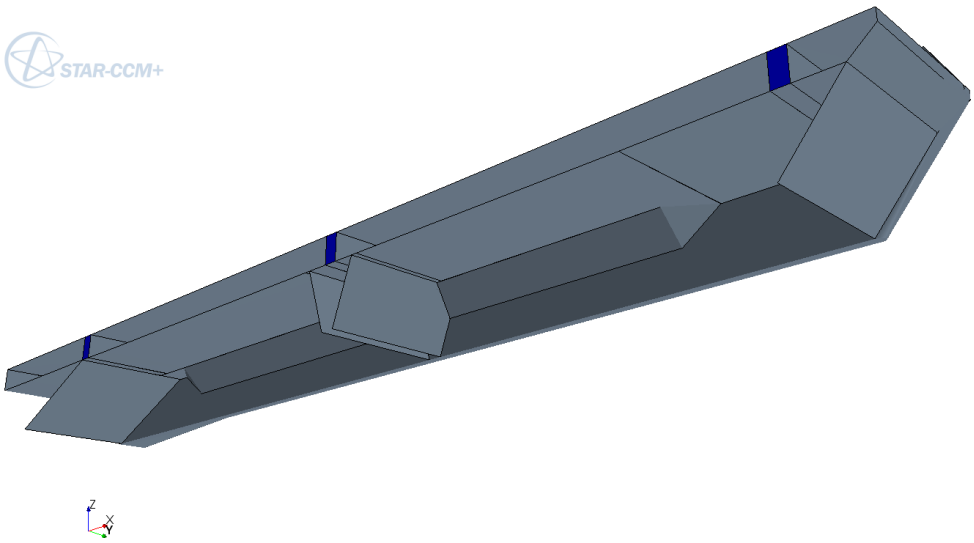

Figure 31: SES with porous skirt implementation.

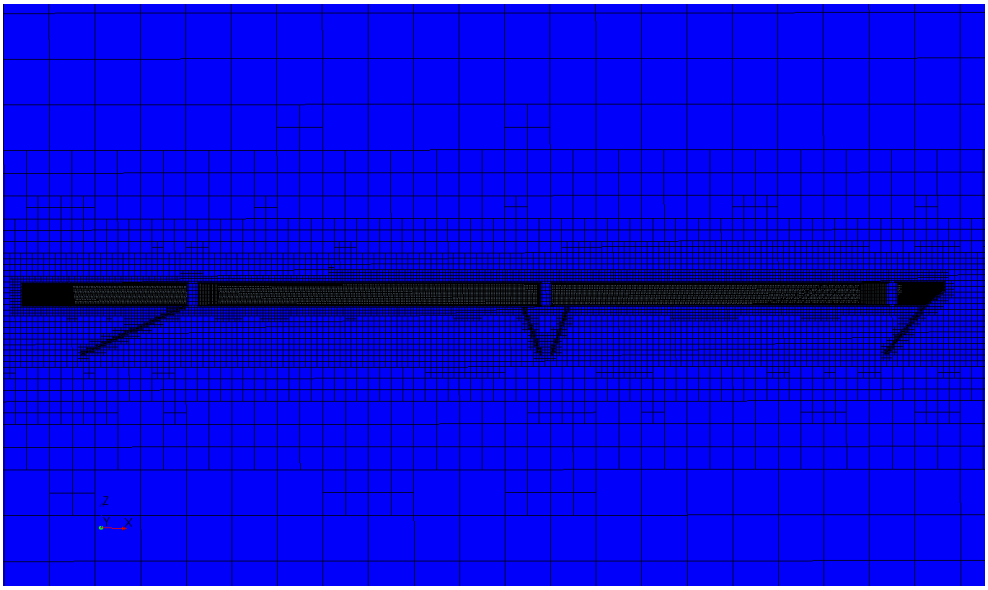

Figure 32: SES with porous skirt implementation mesh.

8.2 SES Porous Skirt Simulations

Implementing these porous skirts on the SES makes the numerical simulation quite complex. The porous skirts were modeled as porous baffle interfaces within STAR-CCM+ which act as an infinitesimal thickness wall. A conformal mesh is then applied to the baffle geometry which assures that volume cells match across the interface. According to the porosity function specified in Equation 5, a porous resistance value is applied to each individual cell on the interface. Given the initial conditions the porous resistance values can be seen Figure 33.

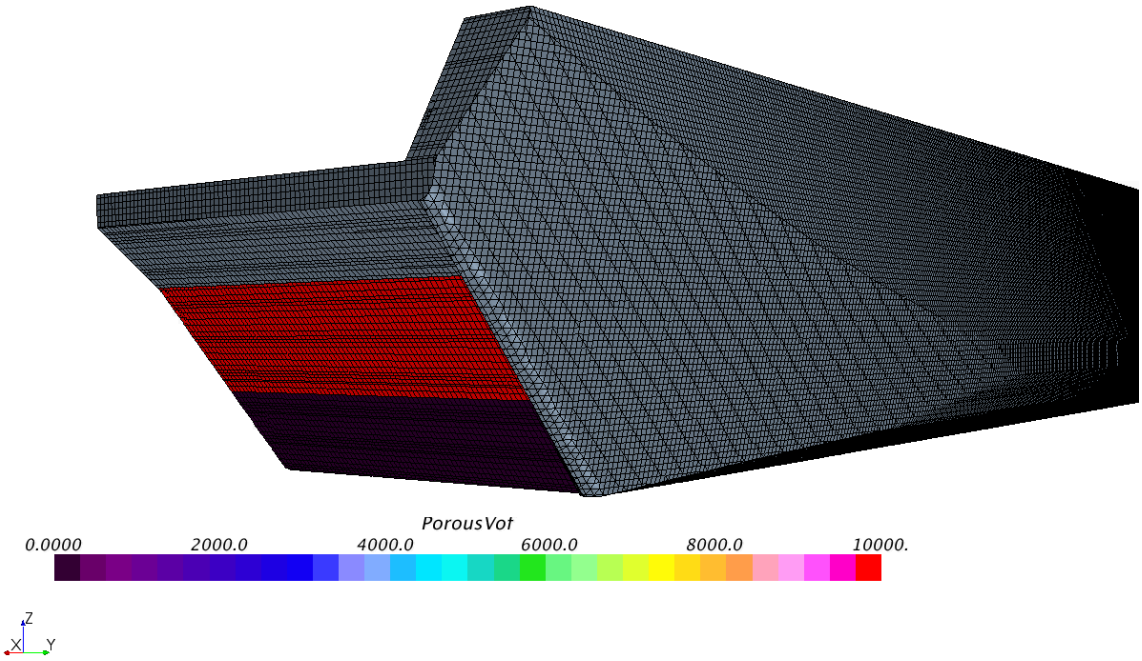

Figure 33: SES front skirt porosity function implementation.

Inviscid simulations involving forward, aft, and transverse porous skirts were first attempted in calm water. Convergence issues immediately arose due to numerical unsteadiness during the initial stages of the simulation. As the craft experienced incoming flow and attempted to stabilize on the pressurized air cushion it began to pitch and heave as expected. This movement caused the skirt interfaces to experience rapid changes in volume fraction of air seen. In turn the porous resistance values changed very quickly which lead to instabilities. As well, the individual cells of the porous skirts saw locally varying volume fractions of air. This developed into a problem due to the small mesh resolution on the waterline and porous interfaces. Two cells that reside geometrically adjacent saw a drastic difference in porous resistance value. These local variations lead to numerical oscillations and unrealistic flow behavior.

To combat this numerical unsteadiness multiple approaches were taken to investigate and correct these issues. A release time was added to the 6-DOF solver to allow time for the fluid flow to develop around the body before he craft was allowed to move. As well, a ramp time was added to the 6-DOF solver to facilitate a more robust solution by reducing oscillatory movements. The ramp causes the forces and moments on the body to be applied proportionally over a time interval to reduce any shock effect on the body. Additionally, the under relaxation factors for the pressure and velocity solvers were examined and manipulated in order to produce a converged solution. All of these methods were successful in helping the SES simulations involving porous skirts to achieve some level of convergence, however, numerical unsteadiness still persisted and an adequate solution was never accomplished.

Future work is needed to provide a desirable simulation involving a surface effect ship with fully porous skirts. This porous skirt model would then need to be validated with comparison to experimental results for both calm water and wave cases.

9. Conclusions and Discussion

Numerical simulations can be used to model real life conditions. In this case a SES model was simulated using the commercial CFD code STAR-CCM+. In order to ensure accuracy of the simulation an adequate grid resolution is required. A grid convergence study was performed using an inviscid simulation in order to determine an adequate mesh resolution. Once an adequately refined computational domain was determined the simulations were run as fully viscous. The turbulent model Spalart-Allmaras was used to solve for the turbulent viscosity and the boundary layer on the hull was resolved by the addition of a prism layer mesh. The drag was monitored for both the inviscid and viscous simulations and then compared. While the pressure drag on the SES is the primary drag source, the shear drag can play a significant role. This lends to the conclusion that viscous turbulent modeling is required in order to accurately predict SES characteristics. The drag for the viscous simulations was also seen to have a distinct oscillatory nature induce by pitch motions. These pitch motions were small in nature but require careful consideration when calculating an average of the drag value. When comparing the viscous drag from the simulations with the SES model test it can be seen that the simulations overestimate the drag. This is primarily due to the approximations of the skirts as rigid. By adding dynamic flexible seals the drag could be more closely approximated.

In addition the ability of CFD to simulate the SES in wave cases was investigated. Initially, the capabilities of STAR-CCM+ to model waves were investigated. It was found that multiple wave models were available including simple sinusoidal wave approximations, superposition of waves, and irregular waves. A simple work boat hull form was run for a regular fifth order wave approximation and irregular wave case. The results including pitch and heave were then compared. As expected the motions in the regular wave case were periodic and sinusoidal when compared with the irregular case which was seemingly random. From this point it was desired to run the full SES simulation in wave cases, however, current skirt approximations within the numerical simulation causes issues. Primarily, the rigid skirts would interact with the free surface causing unrealistic drag and motions. The realistic way to tackle this problem would be to model the skirts as fully dynamic and flexible using a FSI simulation. FSI problems are very difficult and computationally expensive however, and modeling a full SES with multiple flexible skirts is still not feasible. Therefore, an alternative method for modeling SES skirts is desirable in order to simulate wave cases. By means of a user defined porosity function it is possible to model a skirt that would maintain cushion pressure while not interfering with the free surface. Implementing these porous skirts on the full SES geometry proves difficult but future work would lead to simulating a SES in waves.

References

[1] Bishop, R. C., Silver, A. L., Tahmasian, D., Lee, S. S., .Park, J. T, Snyder, L. A., and Kim, J. 2009. "T-Craft Seabase Seakeeping Model Test Data Report", NSWCCD-50-TR–2009/055, Hydro-mechanics Department Report.

[2] Yun, L. and Bliault, A., *Theory and Design of Air Cushion Craft*, Bath Press, Great Britain, 2000.

[3] Maki, K.J., Broglia, R., Doctors, L.J., and Di Mascio, A., "Numerical Investigation of the Components of Calm-Water Resistance of a Surface Effect Ship", Ocean Engineering, 2013, Vols. 72, 375-385.

[4] Bloxom, A., "Numerical Simulation of Fluid-Structure Interaction of a Surface Effect Ship Bow Seal", Ph. D. Dissertation, Virginia Tech, 2014.

[5] Donnelly, D., "Numerical Simulation of Surface Effect Ship Air Cushion and Free Surface Interaction", M.S. Thesis, Virginia Tech, 2010.

[6] Muzaferija, S., Perić, M. " Computation of free surface flows using interface-tracking and interface capturing methods", In O. Mahrenholtz, M. Markiewicz (eds.), *Nonlinear Water Wave Interaction*, Chap. 2, 59-100, WIT Press, Southampton, 1999.

[7] Ferziger, J.H., Peric, M., *Computational Methods for Fluid Dynamics*, Springer, Berlin, Germany, 2002.

[8] Roache, P. J., "Perspective: A Method for Uniform Reporting of Grid Refinement Studies", Journal of Fluids Engineering, Vol. 116, No. 3, 1994.

[9] Roache, P. J., *Verification and Validation in Computational Science and Engineering*, Hermosa Publishers, Albuquerque, NM, 1998.

[10] Oberkampf, W.L., Roy, C.J., *Verification and Validation in Scientific Computing. Cambridge,* Cambridge University Press, 2012.

[11] Veluri, S. P., Roy, C. J., and. Luke, E. A., "Comprehensive Code Verification Techniques for Finite Volume CFD Codes," Computers and Fluids, April 2012.

[12] Donnelly, D. J. and W. L. Neu, "Numerical Simulation of Flow About a Surface-Effect Ship", Proc. 11th International Conference on Fast Sea Transportation, FAST 2011, Honolulu, Hawaii, USA, September 26-29, 2011.

[13] Lin, W., Zhang, S., and Weems, K., “Numerical Simulations of Surface Effect Ship in Waves”, Proceedings 2010 Grand Challenges in Simulation and Modeling, July, 12-14, Ottawa, ON, Canada

[14] Kring, D., et al., “Simulation of Maneuvering in Waves for a High-Speed Surface Effect Ship”, Honolulu, Hi : Proc. 11th International Conference on Fast Sea Transportation, 2011.

[15] Bhushan, S., Stern, F., Doctors, L., “T-Craft Calm Water Resistance and Motions, and Seakeeping in Regular Waves”, Proc. 11th International Conference on Fast Sea Transportation, Honolulu, Hi, 2011.

[16] Donnelly, D. and W.L. Neu, “Numerical Simulation of Surface Effect Ship Air Cushion and Free Surface Interaction”, Proc. 7th Inter. Conf. on High Performance Marine Vehicles, Melbourne, FL, Oct. 13-15, 2010.

[17] CD-adapco/STAR-CCM+8.02.011/help guide